Sensitivity of a tropical montane cloud forest to climate change, present, past and future: Mt. Marsabit, N. Kenya

Sietse O. Los[a], F. Alayne Street-Perrott[a], Neil J. Loader[a], Cynthia A. Froyd[b], Aida Cuní-Sanchez[c], Robert A. Marchant[c]

[a] *Department of Geography, Swansea University, Singleton Park, Swansea SA2 8PP, United Kingdom*
[b] *Department of Biosciences, Swansea University, Singleton Park, Swansea SA2 8PP, United Kingdom*
[c] *York Institute for Tropical Ecosystems, Environment Department, University of York, Heslington, York, YO10 5NG, UK*

Abstract

During the Last Glacial Maximum (LGM) lowland forests contracted throughout the tropics but, by contrast, many montane forest taxa moved to lower elevations. These taxa are often found in cloud forests, which are globally important ecosystems that depend on the capture of atmospheric water from fog drifting through the canopy, here referred to as occult precipitation. Understanding the response of tropical montane taxa to climate variations is limited by a lack of modern data on fog capture; whereas palaeoecological data only provide indirect evidence for its importance. Hence, the response of vegetation to fog capture is not considered in palaeo-estimates of precipitation. We develop a method that uses satellite Normalized Difference Vegetation Index (NDVI) data to estimate the annual amount of occult precipitation and investigate the sensitivity of a cloud forest to past and future changes in both rainfall and occult precipitation. We apply this method using satellite and meteorological data from 1982 to 2015 collected at Mt Marsabit, which is located in northern Kenya (2.34° N, 37.97° E, summit 1707 m a.s.l.). Mt Marsabit has a sub-humid tropical montane cloud forest at its summit that is excessively green for the amount of rain it receives. We estimate the annual amount of occult precipitation for current conditions at about 900 mm y^{-1} which is more than the average annual rainfall of 700 mm y^{-1}. This is consistent with the observation that, for the wider Marsabit

area, interannual variations in NDVI are more closely linked to changes in cloud-base height ($r^2 = 0.87$) than to changes in rainfall ($r^2 = 0.67$). We investigate the sensitivity of forest extent to past and future changes; for the LGM we estimate that cloud-base height decreased by 500 m in response to a 4 °C cooling and that this caused a 20 % to 100 % increase in forest area despite a 30 % decrease in rainfall, a 22 % decrease in atmospheric humidity and a substantial reduction of atmospheric CO_2 levels (values representative for mountains in Kenya during the LGM). An expected increase of 250 m in the cloud-base height associated with a future 2 °C global warming is likely to reduce forest extent by 50 % to 100 %. Our results indicate that the satellite vegetation record is useful to estimate modern hydrological inputs into drier cloud forests (up to 2000 mm y^{-1}) and that this information can be used to estimate the contribution of occult precipitation to altitudinal displacements of tropical montane cloud-forest species during the Quaternary.

Keywords: Climate Change — Tropical Montane Cloud Forest — Normalized difference vegetation index — Occult precipitation — Cloud-base height — Last Glacial Maximum — Data treatment, data analysis — Vegetation dynamics — East Africa

---

The authors declare that they have no competing financial interests

1. Introduction

Tropical montane cloud forests (TMCFs) are important ecosystems that are highly dependent on their ability to capture water from fog or low-level clouds drifting through the forest (Grubb and Whitmore, 1966; Cavelier, 1996; Bruijnzeel et al., 2010); this form of precipitation is here referred to as occult precipitation. TMCFs are home to many rare and endemic plant and animal species and often provide essential ecosystem services to their surroundings. Serious concerns have been expressed about the extent to which global warming will shrink the areas and altitudinal ranges of TMCFs, due to predicted future changes in the vertical structure of the troposphere, including the distribution and elevation of stratiform cloud (Bradley et al., 2004; Williams et al., 2007; Fu et al., 2011; Ohmura, 2012; O'Gorman and Singh, 2013; Oliveira et al., 2014; Helmer et al., 2019). This is the lifting cloud-base hypothesis (Pounds et al., 1999). Future reductions in the geographical and seasonal incidence of fog immersion (often associated with

increased fire incidence) pose particular threats to biological diversity, productivity, hydrological functioning, and survival of many groups of rare and highly specialised organisms, such as epiphytes, bryophytes, amphibians, and insects (Pounds et al., 1999; Still et al., 1999; Foster, 2001; Karmalkar et al., 2008; Hemp, 2009; Bruijnzeel et al., 2010, 2011; Diaz et al., 2014; Lister and Garcia, 2018). Mountain-top extinctions are also a strong possibility on massifs of only moderate height (Bruijnzeel et al., 2011).

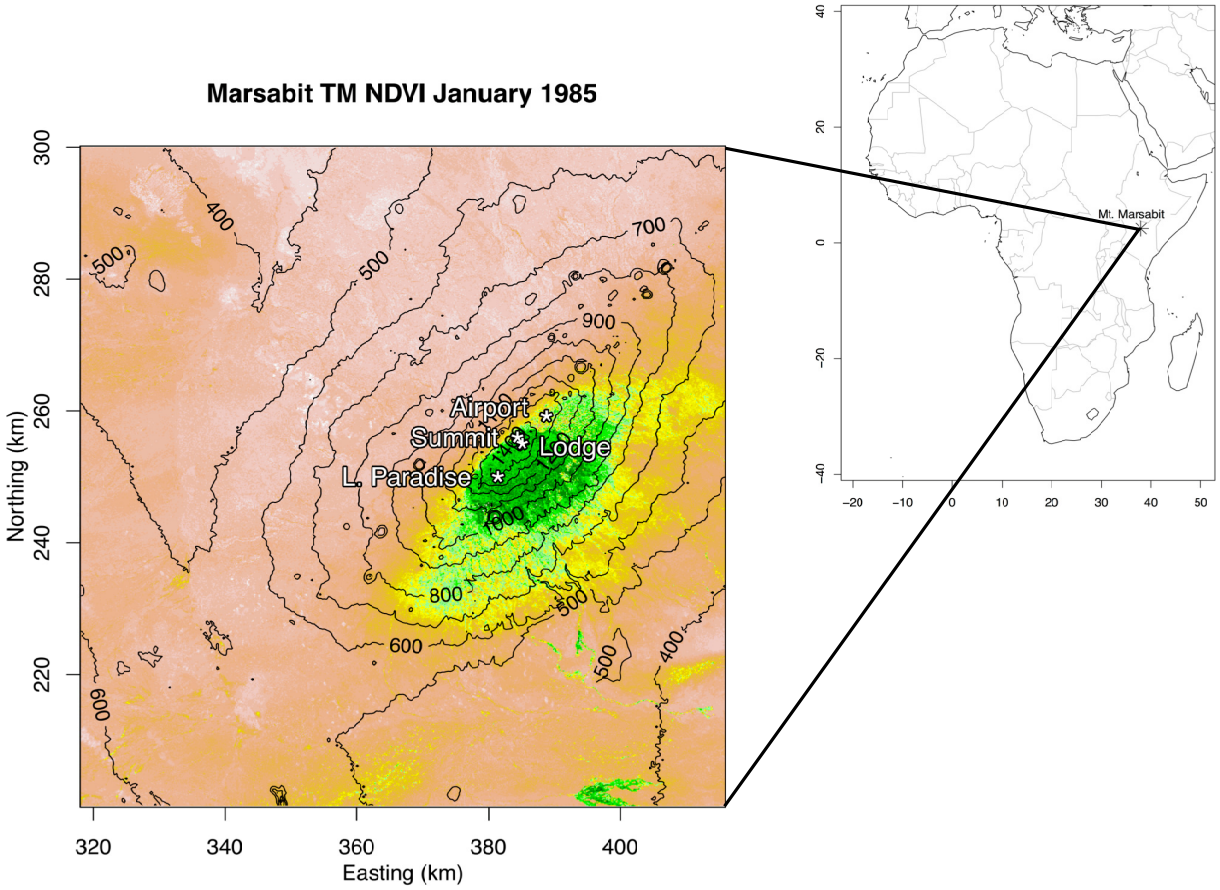

Figure 1: Location of Mt Marsabit (inset) and Landsat 5 NDVI (colour bar) image for January 1985 with contour from the Shuttle Radar Topography Mission (SRTM) (Jarvis et al., 2008). The summit (1707 m a.s.l.), the Marsabit lodge, Marsabit Airport, and Lake Paradise are indicated. (Universal Transverse Mercator projection, zone 37, N)

In contrast, the effects of changes in cloud cover on TMCFs have been largely neglected in Quaternary palaeoclimatology and palaeoecology; there

is, however, a continuing debate about the relative contribution during the Last Glacial Maximum (LGM: ~21ka BP) of the effects on vegetation by changes in air temperature and lapse rate (Van Zinderen-Bakker and Coetzee, 1972; Hamilton, 1982; Bonnefille et al., 1990; Flenley, 1998; Colinvaux et al., 2000; Farrera et al., 1999; Loomis et al., 2017), precipitation (Bonnefille et al., 1990; Bonnefille and Chalié, 2000; Vizy and Cook, 2007), atmospheric CO_2 concentration (Jolly and Haxeltine, 1997; Street-Perrott et al., 1997; Boom et al., 2001; Cowling et al., 2001; Prentice and Harrison, 2009), UV-B radiation flux (Flenley, 1996), wildfire (Wooller et al., 2000; Schüler et al., 2012; Urban et al., 2015; Ivory and Russell, 2016) and herbivory (Ivory and Russell, 2016).

Nevertheless, a few palaeoecologists have speculated about the impact of past variations in stratiform cloud cover and cloud-base height, notably Maley (1987, 1989); Stager and Anfang-Sutter (1999); Marchant et al. (2006); Rucina et al. (2009); Urrego et al. (2010) and Bush et al. (2011). A few pioneering attempts have also been made to model changes in the extent of TMCFs during glacial times (Jolly and Haxeltine, 1997; Wu et al., 2007; Still et al., 1999; Izumi and Lézine, 2016). Unfortunately, these all suffered from relatively coarse spatial resolution and did not consider TMCF - cloud interactions.

Although no palaeo-proxy indicators for persistent montane cloud have so far been discovered, it is possible to infer past changes in its distribution at the LGM, ~21ka BP, from the reconstructed altitudinal descent of pollen taxa characteristic of Upper Montane Cloud Forest and Subalpine Cloud Forest today (terminology follows Scatena et al. (2010)) within the three major tropical rainforest blocs: Africa, Australasia and South America. Prominent examples in different regions include fog-adapted trees and shrubs (Grubb and Whitmore, 1966; Cavelier, 1996; Bruijnzeel et al., 2010) from the families Podocarpaceae (*Podocarpus*, *Dacrycarpus*), Oleaceae (*Olea*), Araucariaceae (*Araucaria*), Fagaceae (*Quercus*), Nothofagaceae (*Nothofagus*), Betulaceae (*Alnus)*, Myricaceae (*Morella*, formerly *Myrica*), Myrsinaceae (*Myrsine*, *Rapanea*), Rosaceae (*Hagenia*, *Polylepis*/*Acaena*) and Ericaceae (*Erica*, *Vaccinium*)(Flenley, 1998). At the LGM, cloud-forest taxa often occupied ecological niches located 300 to >1000 m below their present-day distributions. In the wettest parts of Amazonia (Haberle and Maslin, 1998; Anhuf et al., 2006; Colinvaux et al., 2000; Bush et al., 2011) and Indonesia (Stuijts et al., 1988; Hope and Tulip, 1994; Hope et al., 2004; Pickett et al., 2004), they migrated into areas now occupied by Lowland Rain Forest (LRF). In con-

trast, in drier regions, these fog-adapted elements were restricted to scattered patches within more open, no-analogue plant communities, in association with graminoids (commonly C_4) and savanna/xerophytic trees and shrubs that often have non-overlapping modern distributions (Marchant et al., 2002; Jolly et al., 1997; Street-Perrott et al., 2007; Behling, 1998; Rucina et al., 2009; Hessler et al., 2010; Lézine et al., 2013; Izumi and Lézine, 2016; Lézine et al., 2019). This suggests individualistic species responses to locally prevalent combinations of glacial cooling, reduced rainfall, CO_2-induced physiological drought and/or fewer fog days (implying decreased occult precipitation and a higher solar-radiation flux: see Cavelier (1996)). Enhanced wildfire incidence and grazing pressure may have been important secondary controls.

An additional clue to the palaeoclimatic importance of past variations in montane cloud is provided by the marked contrast between the widespread occurrence of sedimentary hiatuses during the LGM in lowland Amazonia (Ledru et al., 1998) and the continuous sequences obtained from present-day TMCF sites (Bush et al., 2011). From central Kenya to southern Ethiopia, all the Rift lakes, including Lake Victoria and Lake Turkana, were dry or very low prior to the onset of the African Humid Period at ~15ka BP (Junginger and Trauth, 2013; Morrissey and Scholz, 2014; Foerster et al., 2015) whereas continuous sedimentary sequences spanning the LGM have been retrieved from a number of lakes and mires at mid-elevations (Hamilton, 1982; Perrott and Street-Perrott, 1982; Street-Perrott et al., 2004, 2007; Rucina et al., 2009). Some sites, notably Rumuiku Swamp, Mt Kenya (2154 m a.s.l.) (Rucina et al., 2009) and Lake Paradise, Mt Marsabit (1370 m a.s.l; data to be published elsewhere) were actually as wet, or even wetter, than today.

Two major factors hamper quantitative assessments of the impact of climate variations on cloud forests. The first is that in a large number of cases the amount of occult precipitation a forest captures is unknown, although more measurements have become available during the past two decades (Bruijnzeel et al., 2011). The second factor is that precipitation and cloud processes are the predominant sources of uncertainty in global climate modelling (IPCC, 2013). Because of these factors, modelling the response of cloud forests to climate change is very much in its infancy, but it is clearly an area where advance is needed.

We investigate the use of Advanced Very High Resolution Radiometer (AVHRR) and MODerate-resolution Imaging Spectroradiometer (MODIS) NDVI (Supplementary Information) to estimate total precipitation of TMCFs and to estimate their sensitivity to variations in rainfall and occult

precipitation. NDVI is near-linearly related to the amount of solar radiation intercepted by vegetation for photosynthesis (Kumar and Monteith, 1982) and annual mean NDVI has been linked to above-ground growing-season biomass (Tucker et al., 1986; Prince, 1991). NDVI data reflect sensitivity of vegetation to variations in atmospheric CO_2 levels globally, to variations in temperature in mid-to-high latitudes and to variations in precipitation in low latitudes (Myneni et al., 1997; Los, 2013; Zhu et al., 2016). NDVI has been used to measure expansion and contraction of the Sahara in response to annual variations in rainfall (Tucker et al., 1991) and has also been used to identify areas subject to variations in the North Atlantic Oscillation in northern latitudes (Los et al., 2001), and to the El Niño Southern Oscillation predominantly in low latitudes (Myneni et al., 1996; Los et al., 2001).

We test our approach on the TMCF of Mt Marsabit, which is one of the highest mountains in northern Kenya (1707 m a.s.l.; Fig. 1). This region receives rainfall well below 2000 mm y^{-1}, the upper limit of our method. It has a long-term meteorological record from the Marsabit weather station (2.33959 ° N, 37.97314 °E, 1345 m a.s.l.) that overlaps with the NDVI data.

1.1. Vegetation of the Mt Marsabit region

Mt Marsabit is an extinct volcano that forms a so-called island in the desert (Bussmann, 2002); it supports a closed canopy, sub-humid evergreen broad-leaved cloud forest (Grubb, 1977; Bruijnzeel and Proctor, 1995; Bruijnzeel et al., 2011; Githae et al., 2007). Mt Marsabit forms part of the Eastern Afromontane Biodiversity Hotspot (Mittermeier et al., 2004) providing a habitat for a large number of montane species of trees, plants and animals, including several threatened and vulnerable endemic species (IUCN, 2016; Githae et al., 2007), e.g. the Nteroni tree (*Rinorea convallarioides*) and the Marsabit chameleon (*Trioceros marsabitensis*). The vegetation above 1500 m a.s.l. consists of evergreen broad-leaved forest with abundant *Cassipourea malosana* and *Olea capensis*. The NDVI values of this forest, around 0.78, overlap with the highest values of the evergreen xeromorphic forest that is situated at lower altitudes (dominated by *Olea europaea* subsp. *africana* and *Croton megalocarpus*). The lower limit of the xeromorphic forest coincides approximately with a mean annual NDVI value of 0.7. Below 1100 m a.s.l. a thorny bushland grows (dominated by *Commiphora*, *Grewia* and *Acacia*) (Bussmann, 2002) that is surrounded by arid areas such as the Chalbi Desert. Mt Marsabit is one of only a few places in the world where wild populations of *Coffea arabica* (Arabian coffee) are found, a species recently classified as

endangered (Moat et al., 2018, 2019). These wild strains have the potential to increase genetic variety in coffee cultivars and thereby build greater resistance to diseases (Moat et al., 2017; Aerts et al., 2017). Wildlife, in particular elephants, finds a place to obtain food and water when travelling through the hostile, surrounding dry lands (Ngene et al., 2010). For humans, the relatively large amount of precipitation received by Mt Marsabit is an important source of fresh water for livestock and human consumption both for the mountain itself, as well as for its wider region (Cuní-Sanchez et al., 2018).

1.2. Local climate

Mountain summits in the region receive mean annual rainfall of 780 ±370 mm in contrast to an average of 250 ±100 mm in the surrounding lowlands (Cuní-Sanchez et al., 2018). The climate of Mt Marsabit is influenced by seasonal north-south movements of the tropical rainbelt that passes over the area twice per year, resulting in two wet (March–May and October–December) and two dry seasons (January–February and June–September; Fig. 2.a). Variability of rainfall at the Marsabit station is high both within and between years. Mean monthly temperatures vary between 19 °C and 22 °C within the year. This is the optimal range for vegetation growth globally since in this range vegetation is not limited by cold temperatures, high temperatures or high respiration rates (Berry and Björkman, 1980; Chapin, 1980; Ryan, 1991). Variations in monthly temperatures between years are usually smaller than 1 °C (Fig. 2.b). Calculated cloud-base height (Section 2.3.1; eq. 1) decreases during the rainy seasons with average levels close to the summit of Mt Marsabit (Fig. 2.c). The NDVI is high throughout the year with the lowest values occurring at the end of the second dry season (September; Fig. 2.d). Fog occurs throughout the year but is most frequent during the wet seasons (Fig. 2.e and f). The variations in the diurnal cycle of cloud-base height (Fig. 3.a) show minimum values between 0.00 h and 8.00 h which overlap in large part with the occurrence of high humidity (vapour-pressure) values between 3.00 h and 11.00 h (Fig. 3.b). Mt Marsabit receives its moist air and low-level clouds from the Indian Ocean via the Turkana Channel Jet (Kinuthia and Asnani, 1982); the latter is associated with dominant, almost continuous south-easterly winds at Mt Marsabit throughout the year (Fig. 4).

Total precipitation for the summit of Mt Marsabit is greater than the amount of rainfall, since large amounts of water are captured by the forest

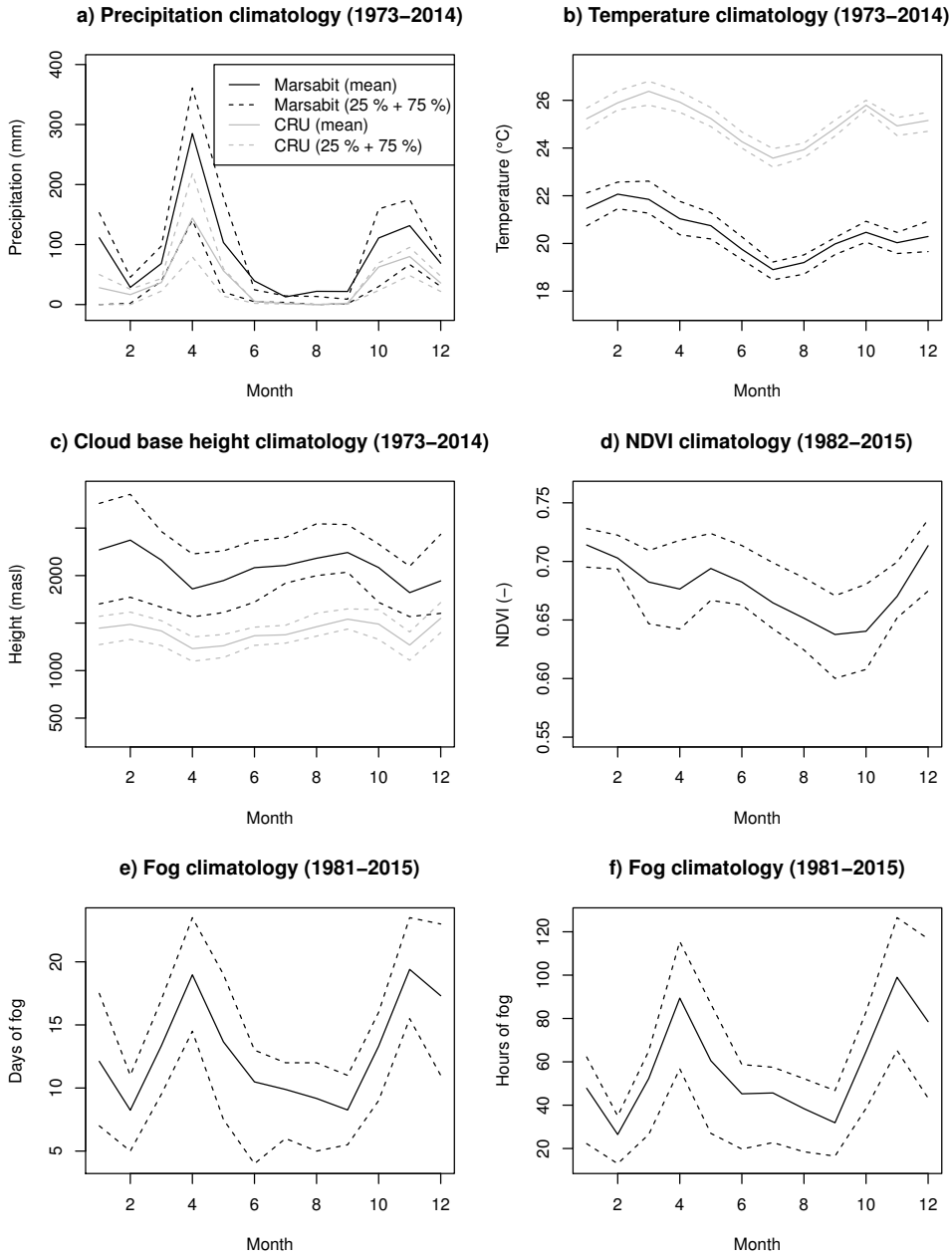

Figure 2: Climatology of Mt Marsabit shown for period over which data are available. a. Mean monthly precipitation with interquartile range (25 % and 75 %) from the Marsabit weather station (1345 m; black lines) and Climate Research Unit (CRU) data (Harris et al., 2014). b. As a. but for temperature. CRU data are representative for a $0.5° \times 0.5°$ cell which includes the dry, hot regions surrounding Mt Marsabit. c. Calculated cloud-base height climatology (eq 1). d. MODIS and AVHRR NDVI climatology for 1982–2014. Seasonality of e. fog days and f. fog hours (Cuní-Sanchez et al., 2018).

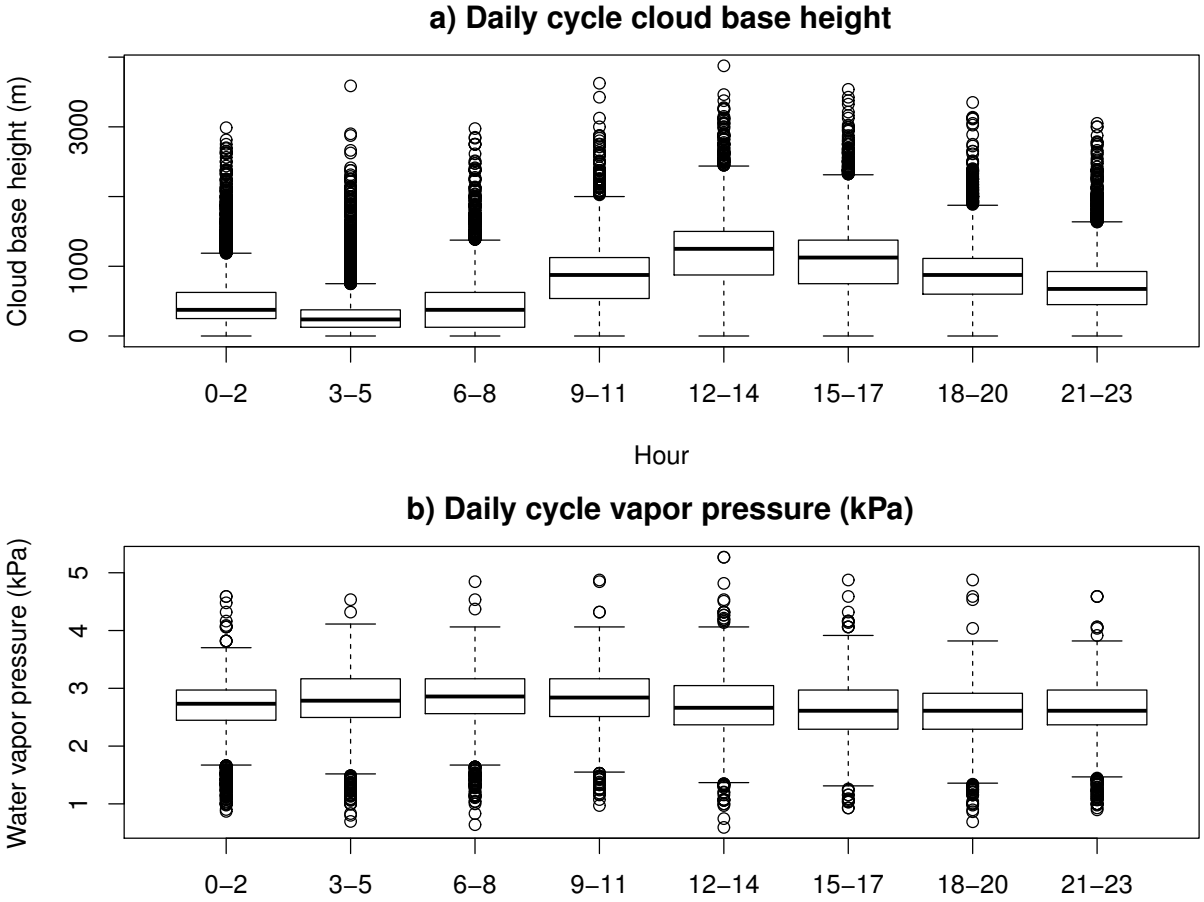

Figure 3: Boxplots (showing median, interquartile range, 2.5 × the interquartile range and outliers) of a. Daily cycle of cloud-base height from data aggregated over 1976–2016 b. Same as a. but for vapour pressure.

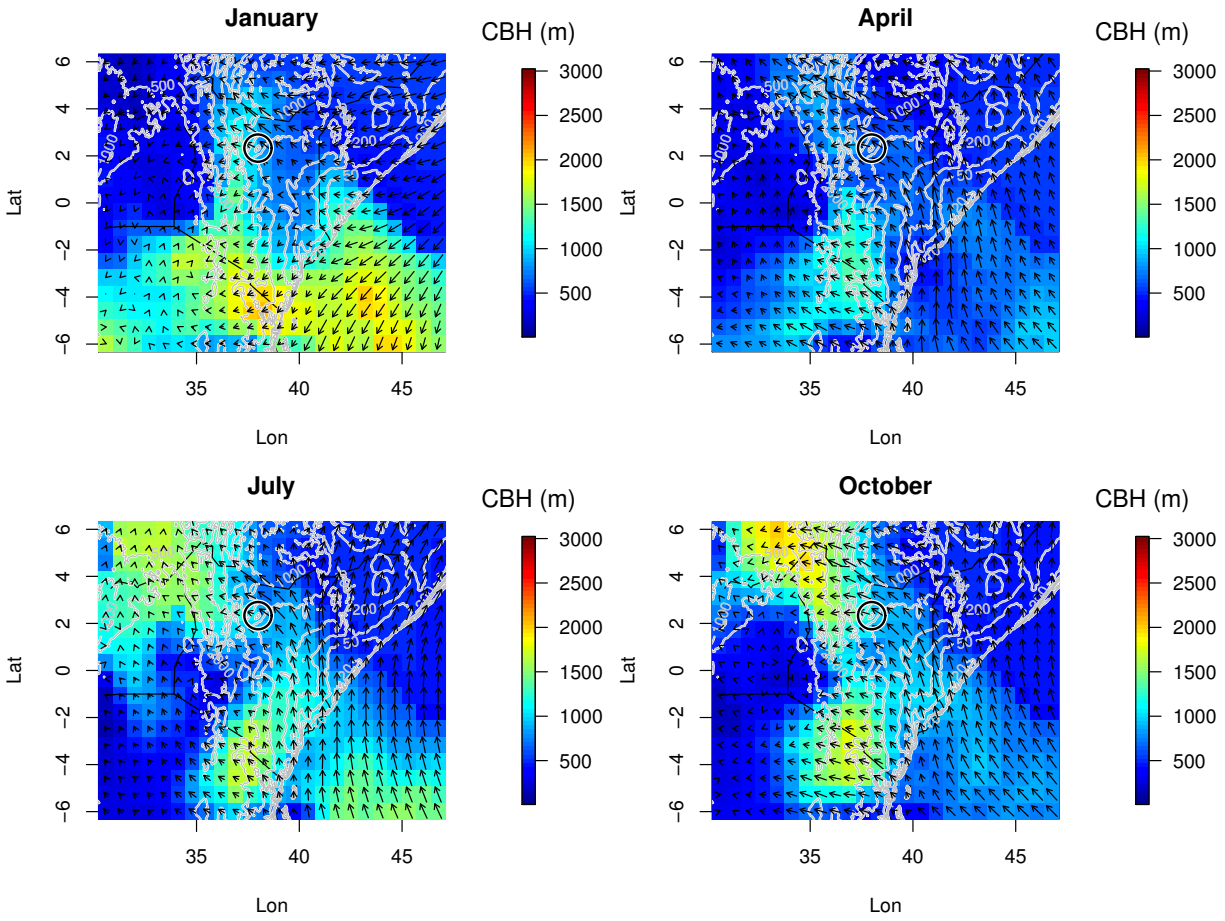

Figure 4: January, April, July and October climatologies of European Centre for Medium-Range Weather Forecasts (ECMWF) Re-Analysis (ERA)-Interim (Berrisford et al., 2011) wind fields (arrows) and cloud-base height (CBH — from ECMWF dewpoint and 2 m air temperature; colour bar) for Kenya. Elevation contours are grey, the black circle shows the location of Mt Marsabit and the black lines show country boundaries. The Turkana Channel Jet flows from the Indian Ocean to Mt Marsabit between the Ethiopian Highlands to the north and the East African Highlands to the south.

canopy from low-level clouds; the resulting fog drip from the canopy frequently generates overland flow along roads and other impermeable surfaces during the rainy season (Muchura et al., 2014). Measurements of fog capture were made during a number of field campaigns in the Marsabit forest using a vertical mesh at altitudes of 1450 and 1500 m a.s.l. Highest values occurred during the rainy season; total annual values were between 250 to 350 mm (Nicholson, 1936; Muchura et al., 2014; Cuní-Sanchez et al., 2018). Mesh-based measurements of fog provide an indication of its variability within and between years, but are difficult to translate to rainfall-equivalent vertical precipitation. Analyses of oxygen and hydrogen isotopes also indicate a substantial contribution of fog drip to groundwater on Mt Marsabit (Ingraham and Matthews, 1988), although this is difficult to quantify due to the lack of modern rainfall-isotope data.

The water supply to the summit of Mt Marsabit has diminished over the last few decades. Rainfall decreased from 1961 to 2010 by about 10 mm annually (Dabasso and Okomoli, 2015) and the number of days with fog has declined by about 50% over the past three decades (Cuní-Sanchez et al., 2018). Cutting of trees, e.g. for cattle fodder, has reduced the ability of the forest to capture occult precipitation (Martínez et al., 2009; Cuní-Sanchez et al., 2018); demand for groundwater has also increased pressures on the forest and curtailed its ability to capture occult precipitation.

In summary, fog capture is an important component of precipitation on Mt Marsabit, but its total amount has not been quantified. Furthermore, there is evidence that fog capture has decreased over the past decades and that this has contributed to a decline in forest extent. Diminished fog capture associated with climate change and land management may have had a significant impact on the water balance of the Marsabit TMCF but its magnitude is largely unknown. The present study therefore aims to address the following questions:

1. How much does occult precipitation contribute to modern total precipitation?
2. How sensitive is the forest to colder and warmer climatic regimes, e.g. at the LGM and resulting from global warming?
3. How important are the separate contributions of occult precipitation and rainfall to the forest during colder and warmer climatic regimes?

Materials and Methods are described in Section 2. In Section 3 the sensitivity of the TMCF to present, future and past climate change is estimated.

The discussion is found in Section 4. In Supplementary Information we provide details of the NDVI data, an error analysis of our estimates of occult precipitation on Mt Marsabit, details on the models used to estimate the sensitivity of the Marsabit TMCF to climate change, and an alternative sensitivity simulation of the Marsabit TMCF for the LGM and for a global warming scenario.

2. Materials and methods

2.1. Modern meteorological data

Marsabit station data. (1976–2015; location: 2.33959°N, 37.97314 °E; 1345 m a.s.l.) We obtained Marsabit meteorological data — cloud cover, surface air temperature, dew-point temperature, wind speed, visibility and past weather (fog) observations — from the National Oceanic and Atmospheric Administration (NOAA) National Climatic Data Center (NCDC) Integrated Surface Data set (ISD; Smith et al. (2011)). Monthly statistics of daily and hourly fog occurrence and monthly rainfall amounts from the same station were obtained from the Kenya Meteorological Service.

Data from the Marsabit forest. Rain-gauge measurements from the forest were collected by ACS at the Marsabit Lodge for three rainy seasons between October 2014 and December 2015.

Global databases. Tropical rainfall monitoring mission (TRMM) 3B43 monthly precipitation data version 7 (Huffman et al., 2007, 2010) for 1998–2015 at 0.25° by 0.25° resolution were obtained from the NASA Goddard Earth Sciences Data and Information Services Center (GES DISC) Mirador server (http://mirador.gsfc.nasa.gov) to compare with the Marsabit station data. Climate Research Unit of the University of East Anglia (CRU) monthly time series version 3.23 global precipitation, temperature and humidity data at 0.5° by 0.5° resolution (Harris et al., 2014) for 1971–2014 were obtained from the British Atmospheric Data Centre (BADC).

ECMWF reanalysis (ERA-Interim: 1979–2012). ERA-Interim wind fields and cloud-base height at 80 km resolution were obtained from the European Centre for Medium-Range Weather Forecasts (ECMWF) (Berrisford et al., 2011). These data were used to obtain information on wind circulation for the wider area (Fig. 4).

2.2. Satellite land-surface data

NDVI from the AVHRR (1982–1999) and MODIS (2000–2015). AVHRR NDVI data at 8 km resolution were obtained from the Pathfinder AVHRR Land project (James and Kalluri, 1994). A range of corrections was applied to these data to ensure consistency over time and to minimise distortions associated with cloud contamination, aerosol contamination and changes in illumination and viewing angle (Supplementary Information; Los et al. (2000, 2005)). We obtained AVHRR data for the Marsabit forest by selecting the maximum NDVI of a 3 by 3 pixel window centred at the summit; these data were fused with MODIS Terra 1 km data averaged to 8 by 8 km. For the analysis of the wider region, including the analysis of forest extent during the LGM and for a 2° global warming, we used 250 m MODIS 16-day NDVI data. MODIS data were obtained from the United States Geological Survey (USGS) and were interpolated to a monthly time step (Supplementary Information).

SRTM. We used Space shuttle Radar Topography Mission (SRTM) data from the consortium for spatial information (Jarvis et al., 2008) to account for altitude-dependent variations in rainfall and occult precipitation.

HYDE. The HistorY Database of the global Environment (HYDE) land-cover version 3.1 data for 1990 (Klein Goldewijk et al., 2010) were used to identify areas where vegetation was affected by humans (Section 2.3.2).

2.3. Methods

2.3.1. Cloud-base height

Cloud-base height (z_C) or lifting condensation level is the height above the surface at which the the atmosphere becomes moisture-saturated under adiabatic conditions. A good approximation is Espy's equation which is accurate within 2 % for relative humidity values above 50 % and temperatures between 0 °C and 30 °C (Lawrence, 2005):

$$z_C = 125(T_a - T_d), \quad (1)$$

with T_a being the 2 m air temperature and T_d the dew-point temperature (both in K or °C). Throughout the paper we use calculated cloud-base height based on Marsabit weather data.

2.3.2. Estimation of total and occult precipitation

A relationship between annual precipitation and mean annual NDVI is obtained for the tropics (23.5° S – 23.5° N) from 1982–1999 0.5°×0.5° monthly AVHRR NDVI data (Los, 1998; Los et al., 2000, 2005) and CRU TS 3.10 precipitation data (Harris et al., 2014) (Fig. 5). Data from areas with more than 33 % agriculture or grassland as identified in the HYDE version 3.1 data for 1990 (Klein Goldewijk et al., 2010) are removed to minimise the contribution of areas affected by land-cover change. A relationship is estimated between the median NDVI and median precipitation of 41 equidistant intervals from 0 mm y^{-1} to 2000 mm y^{-1}; the regression is weighted by the number of observations in each interval (Fig. 5):

$$P_T = \beta_0 + \beta_1 V \tag{2}$$

with P_T being the annual total precipitation (mm), V the mean monthly NDVI, and $\beta_0 = -120.9$ and $\beta_1 = 2690.4$ the regression coefficients. Occult precipitation is estimated by:

$$P_F = P_T - (P_R + E_O), \tag{3}$$

with P_F being the occult precipitation from fog capture, P_R the rainfall and E_O the underestimate in precipitation introduced by the orographic effect.

2.3.3. Sensitivity of vegetation to changes in cloud-base height and rainfall

The spatial and temporal associations of 250 m MODIS NDVI data (Huete et al., 2002) with the Marsabit station rainfall data and cloud-base height calculations are explored by calculating partial correlations for different time lags; lags for NDVI are varied from $-1.0, -0.5$to 0 months and lags for precipitation and cloud-base height are varied from $-4, -3, -2 - 1$to 0 months. Maximum partial correlations are obtained for precipitation at zero month lag and cloud-base height leading by 1 month; these lags are used in the regression analyses below. Associations between temperature and NDVI are not significant and are therefore not incorporated in the analysis (Table 2).

2.4. Sensitivity of vegetation to climate change

Two regression methods are used to simulate changes in NDVI as a function of cloud-base height and rainfall (Supplementary Information).

2.4.1. Method 1: local regression model

The local model develops a regression equation for each 250 m pixel predicting monthly NDVI as a function of monthly rainfall concurrent with NDVI and mean monthly cloud-base height leading NDVI by one month (Section 2.3.3). Rainfall and cloud-base height are obtained from the station data, NDVI varies spatially. The regression coefficients vary spatially and take into account spatial variations in rainfall and cloud-base height. The local regression provides realistic estimates of NDVI for current conditions but is probably insensitive in areas where variability in NDVI data is small, e.g. the summit of Mt Marsabit which has high NDVI values throughout the year and the surrounding drylands which have consistently low values.

2.4.2. Method 2: regional regression model

The regional model develops one regression equation for the entire region estimating monthly NDVI as a function of monthly rainfall at zero lag and mean monthly cloud-base height with a one month lead (Section 2.3.3) and incorporates in addition the effects of height, location and interactions between variables. The model estimates 23 regression coefficients to simulate spatial and temporal variability of the NDVI (Supplementary Information). The regional model is more sensitive to changes in rainfall and cloud-base height at the summit of Mt Marsabit and in the surrounding drylands.

2.4.3. Altered climates: sensitivity studies

The equations for the local and regional regression models (Supplementary Information) allow estimation of the sensitivity of NDVI to changes in cloud-base height and rainfall. Cloud-base height changes in response to surface air temperature and dew-point temperature (eq. 1). The latter is assumed constant since the trend over time in dew-point temperature at the Marsabit weather station is not significant, but its value can be adjusted, e.g. to obtain changes in cloud-base height projected by climate simulations.

Last Glacial Maximum. During the LGM the decrease in tropical land temperatures was larger for higher altitudes than for lower altitudes (Webb et al., 1993; Farrera et al., 1999). An expression for the change in lapse rate during the LGM compared to current conditions is obtained from the data for East Africa collected by Loomis et al. (2017):

$$\Delta T \quad = \quad -2.88 - 0.00092h, \tag{4}$$

with ΔT being the difference in temperature between the LGM (K or °C) and the present, and h the elevation (m). The equation predicts a decrease in temperature at 1200 m a.s.l. of about 4 °C, which results in a 500 m decrease in cloud-base height (eq 1). We assume a reduction in rainfall of 30% in line with estimates from palaeodata and climate simulations for East Africa (Bonnefille and Chalié, 2000; Hostetler and Clark, 2000). The contribution to precipitation associated with cloud-base height is reduced by 22 % in line with a reduction in saturated atmospheric moisture as a result of a decrease in temperature of 4 °C. We use relationships between temperature and atmospheric humidity as published in Jones (1992). NDVI is reduced by 20% as a result of lower atmospheric CO_2 concentrations (Los, 2013).

Global warming. The effect of global warming is set to 2 °C at 1200 m and dewpoint temperature is held constant which results in an increase in calculated cloud-base height of 250 m. No adjustments are made for changes in lapse rate, rainfall, atmospheric moisture or atmospheric CO_2.

3. Results

3.1. Estimation of total and occult precipitation

The mean annual total precipitation estimated from NDVI (eq 2) is 1700 mm (± 265 mm; precipitation amounts are rounded to the nearest 100 mm). Mean annual rainfall at the weather station (1345 m a.s.l) is 700 mm; we estimate that rainfall for the forest above 1500 m a.s.l. is 73 mm y^{-1} more (Table 1 in Supplementary Information) and estimate occult precipitation at 900 mm y^{-1} (± 265 mm y^{-1}) (eq. 3). Sources of error associated with the effects of fog — a reduction in evapotranspiration and a reduction in NDVI caused by lower photosynthetic rates — are both in the order of 100 to 200 mm y^{-1} but are of opposite sign and effectively cancel each other out (Supplementary Information).

3.2. Interannual variability in climate data and NDVI

Variations in annual total precipitation estimated from NDVI are compared with rainfall from three different data sets for validation (Fig. 6). The rainfall data sets are: 1) local meteorological observations from the Marsabit weather station for 1975–2015; 2) the CRU gridded data (Harris et al., 2014) for 1973–2014 and 3) the TRMM data (Huffman et al., 2007, 2010) for 1998–2015. Closer inspection of the rainfall data shows that the CRU data exhibit

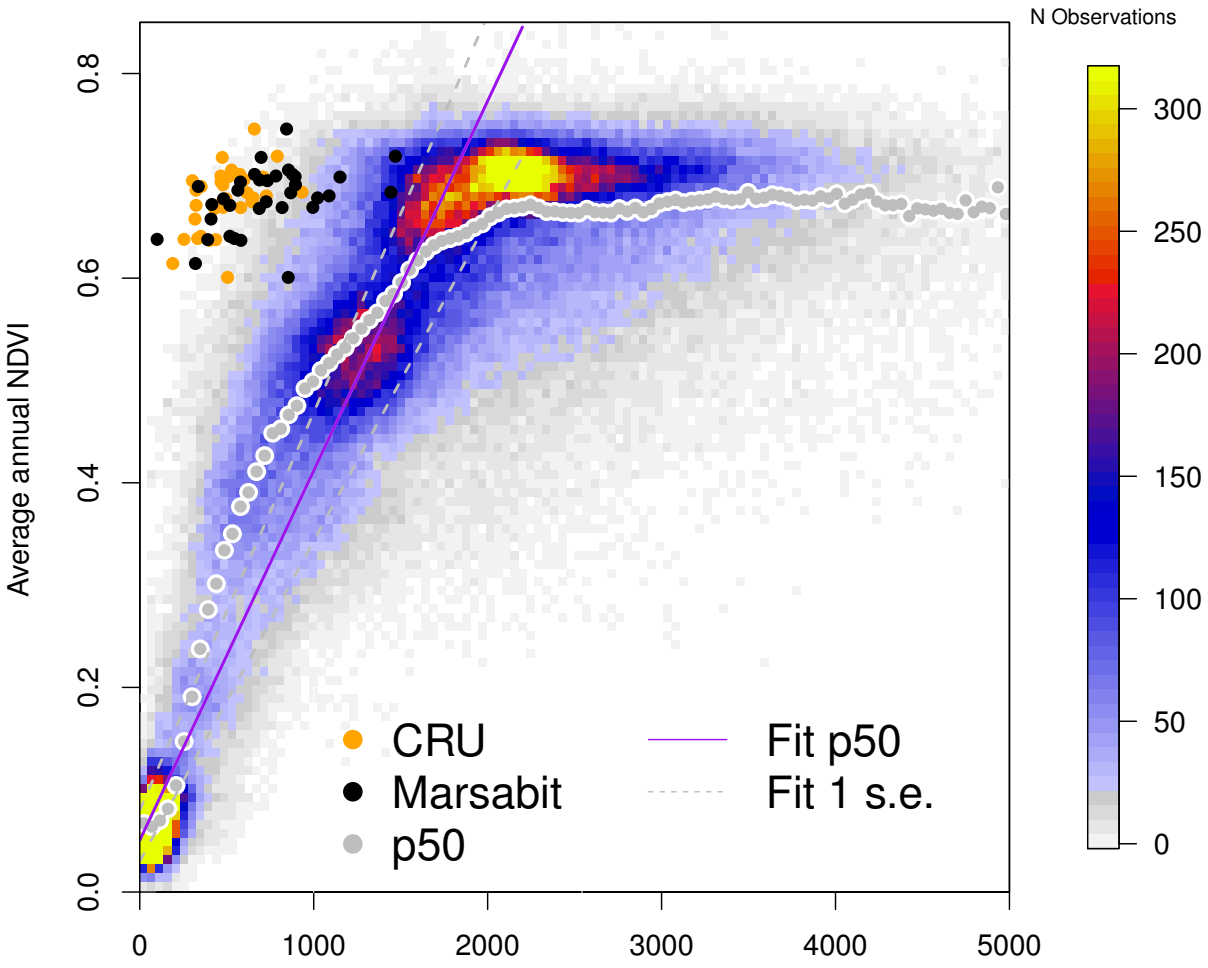

Figure 5: Relationship between CRU precipitation (Harris et al., 2014) and NDVI (V) (Los et al., 2000, 2005) for the tropics (between 23°S and 23°N) and between rainfall and NDVI for Mt Marsabit (orange dots – CRU data; black dots – Marsabit station data). Rainfall above 5000 mm and corresponding NDVI data are not shown. NDVI data from areas with more than 33 % grassland or agricultural land as identified in the HYDE 3.1 data (Klein Goldewijk et al., 2010) are not used for analysis. The standard error of the relationship at 2000 mm is ± 265mm (+ 180 mm and -350 mm); equivalent to a 13 % relative error. The colour bar indicates the number of observations in each x and y interval.

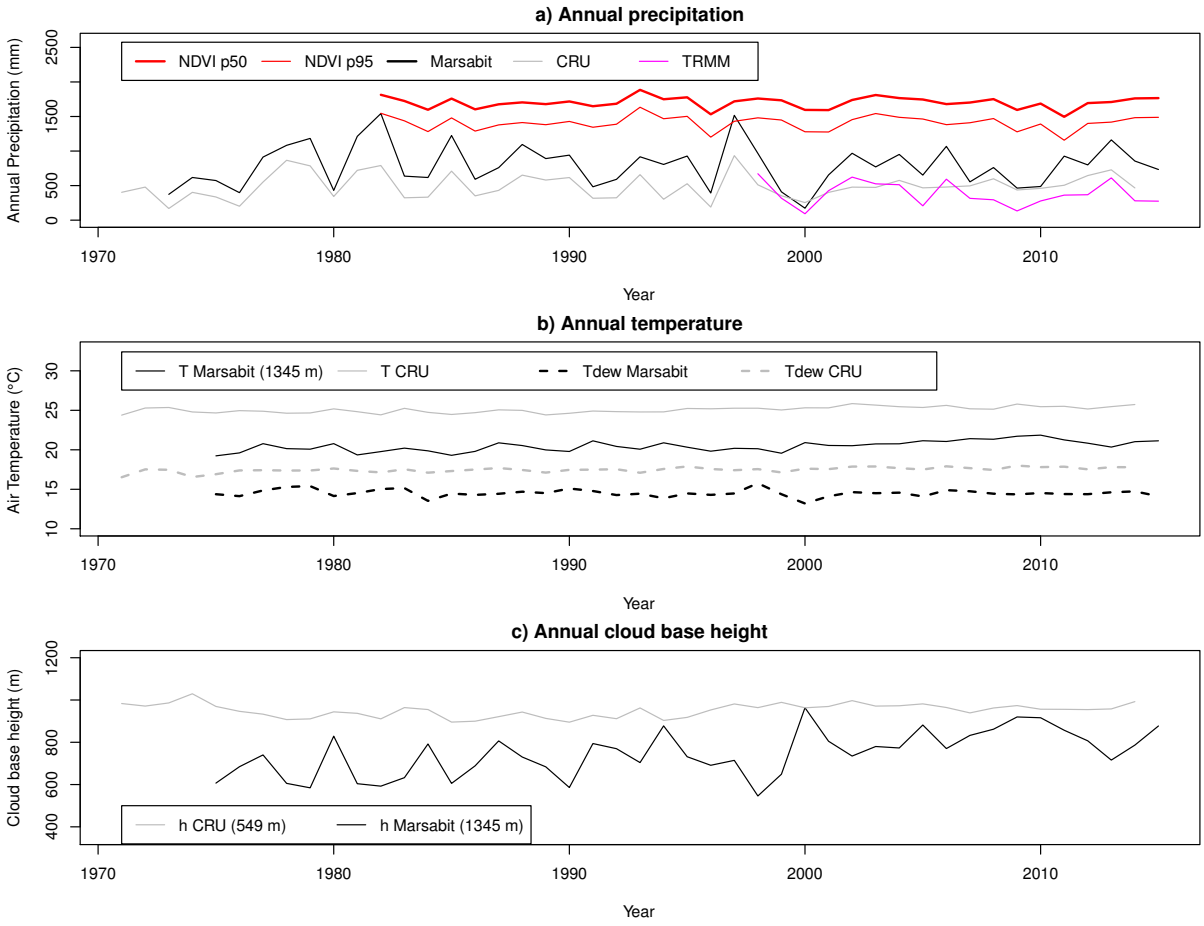

Figure 6: Annual climate time series for Mt Marsabit since 1971. a. Rainfall time series from Mt Marsabit weather station (black), CRU data (grey), TRMM (purple) and total precipitation calculated from NDVI (thick red line); the lower red line shows the 95^{th} percentile. The rainfall measured at Marsabit is increased by 73 mm to representative of orographic effects. b. Annual surface air temperature and dew-point temperature from Marsabit and CRU data. c. Calculated annual cloud-base height (eq. 1) for Marsabit and CRU. Trends are shown in Table 1. CRU data are representative for a $0.5° \times 0.5°$ cell which includes the hot, dry regions surrounding Mt Marsabit.

low variability after 2000; this was probably caused by a decrease in the number of meteorological stations available (Harris et al., 2014). The variability in the Marsabit station data agrees well with the CRU data prior to 2000; and with the TRMM data for its entire record. The total precipitation estimates are substantially higher than any of the rainfall observations on Mt Marsabit; this difference is larger than differences between the rainfall observations (Fig. 6).

Table 1: Trends in annual rainfall, temperature, cloud-base height and NDVI for Mt Marsabit 1973–2014 and 1982–2014. P: rainfall, T_a: air temperature, T_d: dew-point temperature, z_C: cloud-base height. Marsabit refers to Marsabit weather station data and CRU to CRU data. (significance levels: * ($p < 0.1$); ** ($p < 0.05$); *** ($p < 0.001$); NS: trend not significant; –: missing data

	1973–2014	1982–2014
P Marsabit	NS	-11.2 mm y^{-1}*
P CRU	NS	NS
T_a Marsabit	0.04 °C y^{-1} ***	0.04 °C y^{-1}***
T_a CRU	0.02 °C y^{-1}***	0.03 °C y^{-1}***
T_d Marsabit	NS	NS
T_d CRU	0.015 °C y^{-1}***	0.02 °C y^{-1} ***
z_C Marsabit	5 m y^{-1} ***	6 m y^{-1}***
z_C CRU	0.75 m y^{-1} *	2 m y^{-1}***
NDVI	–	NS

Significant linear trends between 1973 and 2014 are found in several of the climate data sets: a small trend is found in the Marsabit rainfall data between 1982 and 2014, whereas more significant trends are found in the CRU and Marsabit annual-mean surface air (2 m) temperature, the CRU annual-mean dew-point temperature, and the CRU and Marsabit annual mean cloud-base height (Fig. 6, Table 1). The trend for 1973–2014 in cloud-base height and air temperature in the Marsabit station data is larger than in the CRU data. Interannual variability in NDVI, and by inference in total precipitation, is positively correlated with rainfall and negatively correlated with cloud-base height. Temperature is not significantly correlated to NDVI, hence its direct effect is not considered in further analysis. The negative correlation between days of fog per year and cloud-base height is larger than that for hours of fog per year (Table 2), possibly indicating variations in the number of observations per day over time.

Table 2: Correlations between annual climate time series, 1982–2015 (1982–2014 for CRU time series); significance levels: ^{a}: $p < 0.1$; ^{b}: $p < 0.05$; ^{c}: $p < 0.001$. NDVI correlates significantly with precipitation and cloud base height. V: NDVI, P: Precipitation, T_a: surface air temperature, T_d: dew-point temperature, z_C: cloud-base height, subscript M refers to measurements from Marsabit and subscript CRU to CRU measurements. Fog days and fog hours are from Marsabit.

r	V	P_{M}	P_{CRU}	$T_{a,\mathrm{M}}$	$T_{a,\mathrm{CRU}}$	$z_{C,\mathrm{M}}$	$z_{C,\mathrm{CRU}}$	fog days
P_M	0.46^b							
P_{CRU}	0.49^c	0.86^c						
$T_{a,M}$	-0.11	-0.31^a	-0.16					
$T_{a,\mathrm{CRU}}$	-0.12	-0.17	-0.14	0.64^c				
$z_{C,\mathrm{M}}$	-0.29^a	-0.49^b	-0.33^a	0.86^c	0.47^c			
$z_{C,\mathrm{CRU}}$	0.02	-0.14	-0.03	0.38^b	0.78^c	0.29		
fog days	0.14	0.21	0.12	-0.61^c	-0.65^c	-0.62^c	-0.45^c	
fog hours	-0.13	-0.14	-0.27	-0.46^c	-0.64^c	-0.39^b	-0.49^c	0.75^c

3.3. Sensitivity of vegetation to changes in cloud-base height and rainfall

3.3.1. Temporal changes in the forest

Variations in the annual NDVI averaged over the wider Marsabit area (Fig. 7) are more closely linked to calculated variations in cloud-base height ($r^2 = 0.87$), than to variations in annual rainfall ($r^2 = 0.67$), confirming the importance of clouds as a source of water in the area.

3.3.2. Spatial dependency of NDVI on rainfall and cloud-base height

The spatial and temporal associations of NDVI with precipitation (zero-month lag) and cloud-base height (1-month lead) for the Marsabit region are shown in Fig. 8. Partial negative correlations with NDVI are larger in magnitude for cloud-base height than for rainfall for the higher parts of the upwind south-east slope and the summit of Mt Marsabit (Fig. 8.c). Precipitation has the highest correlations on the lower parts of the upwind east slope and most of the leeward west slope (Fig. 8.a and 8.c); note that fog does not occur on the leeward side of the mountain.

3.4. Estimation of climate-change sensitivity

Both regression models show the greatest change in NDVI on the slopes of Mt Marsabit below its summit; the mean NDVI value at the summit (above 1300 m a.s.l) shows a small negative change in the local regression model

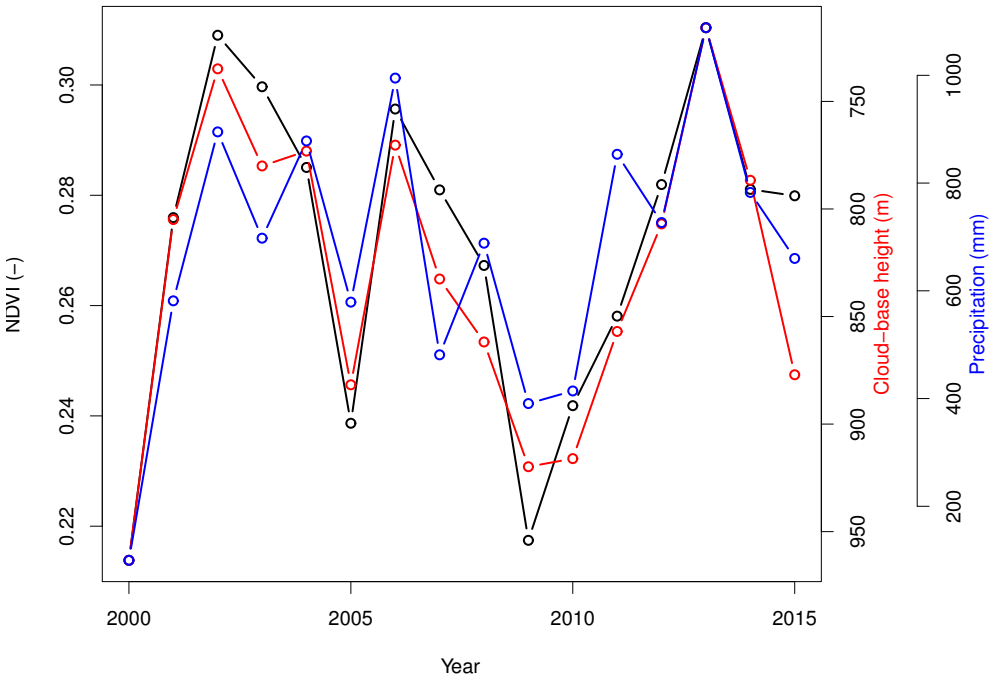

Figure 7: Comparison of annual precipitation and mean cloud-base height (shown in Fig. 6) measured at Marsabit station and the mean NDVI for the wider region of Mt Marsabit (shown in Fig. 8). The axis for cloud-base height is reversed for easier comparison.

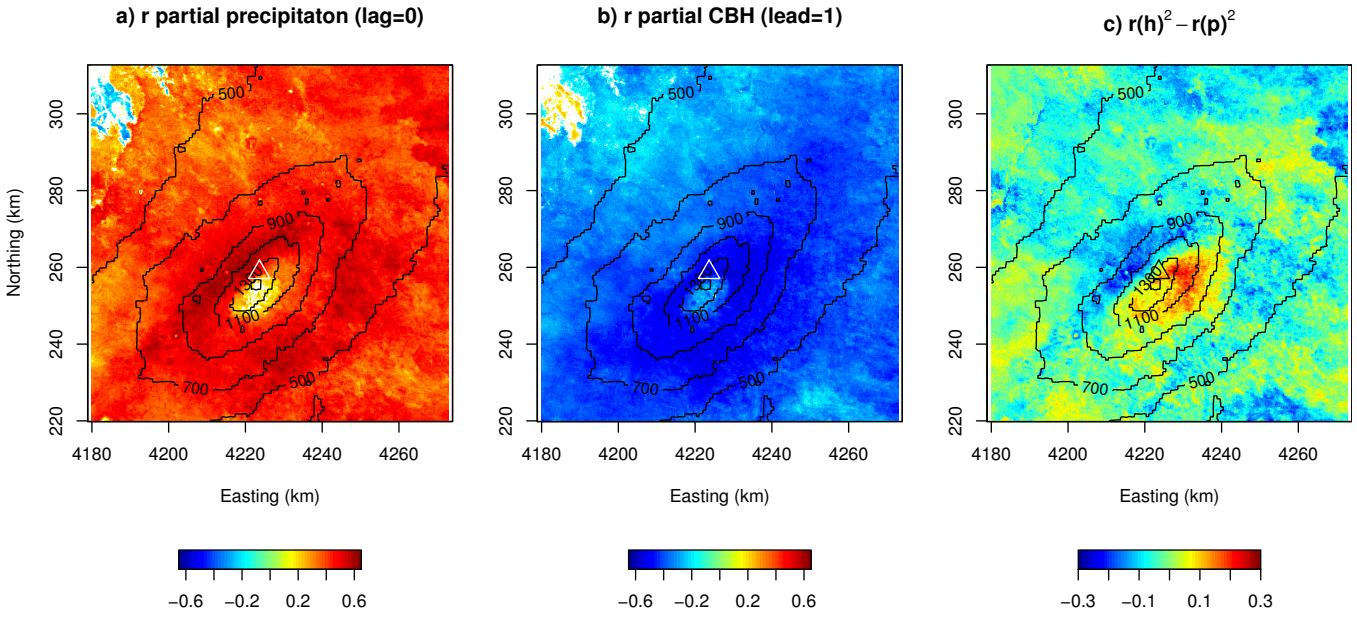

Figure 8: Partial monthly correlations of NDVI with monthly (zero lag) rainfall (a) and calculated monthly (1 month lead) cloud-base height (eq. 1; b). Values that are not significant ($p > 0.1$) are white. c. Difference in r^2 of a. and b. showing that more variance is explained by cloud-base height for the upwind slope and by rainfall for the leeside. (Sinusoidal projection; Easting — distance (km) from the Greenwich meridian; Northing — distance (km) from equator. The triangle indicates the location of the Marsabit weather station)

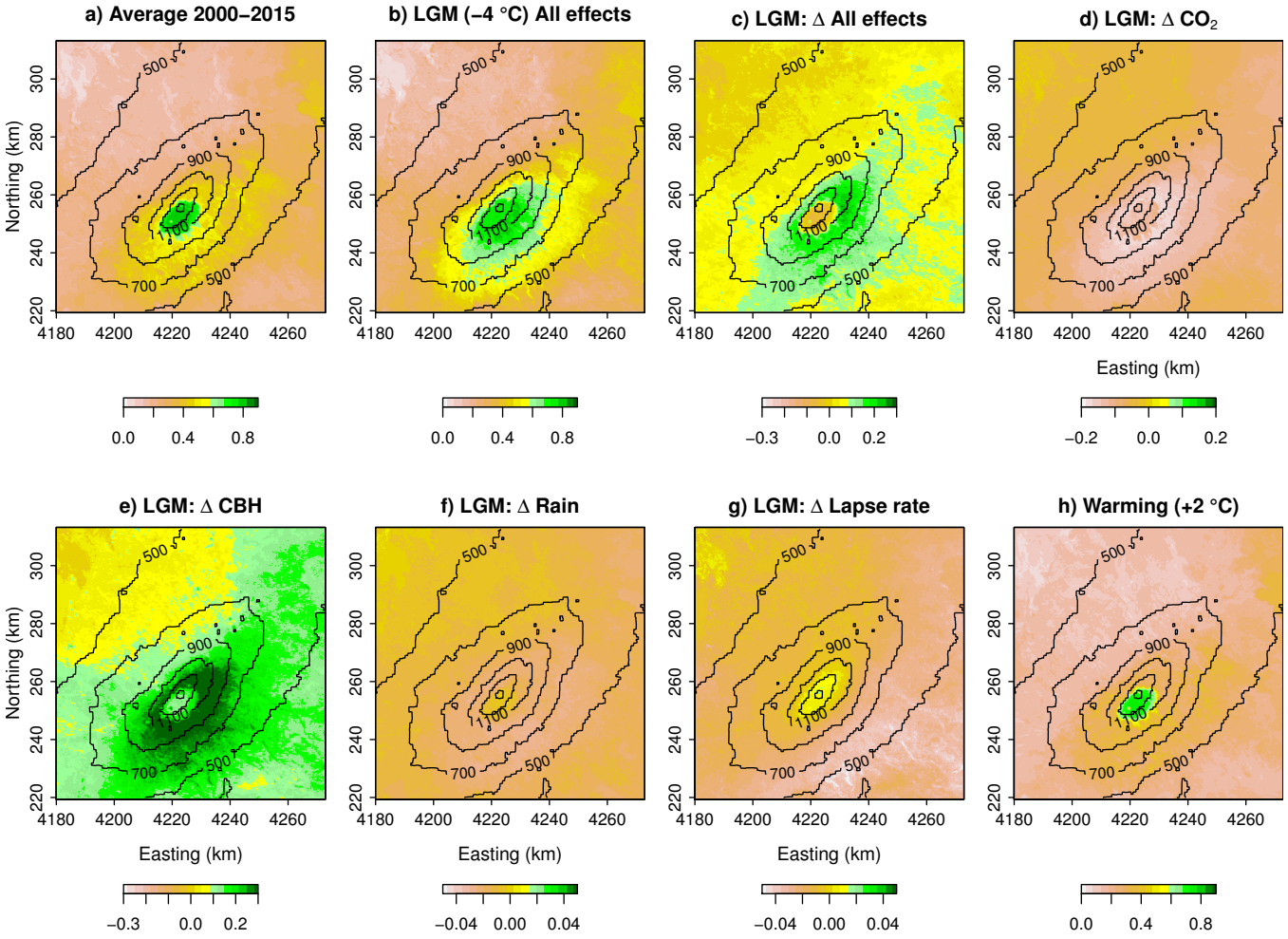

Figure 9: Sensitivity of NDVI to climate change. a. Average NDVI of the Marsabit region for 2000–2015. NDVI = 0.7 approximately coincides with the boundary of the xeromorphic forest. b. Projected NDVI during the LGM using a local regression model with 20 % lower NDVI caused by lower atmospheric CO_2 concentrations, 500 m lower cloud-base height (eq 1) and 22 % lower atmospheric humidity, 30% less rain, and changed lapse rate for the LGM. c. Change NDVI for the LGM compared to current conditions (b. - a.). d. Change LGM NDVI caused by lower atmospheric CO_2 concentrations. e. Change LGM NDVI caused by lower cloud-base height. f. Change in LGM NDVI caused by reduced rainfall. g. Change in LGM NDVI caused by a change in lapse rate (Loomis et al., 2017). h. Projected NDVI resulting from a 250 m increase in cloud-base height caused by 2 °C warming. (Sinusoidal projection; Easting — distance (km) from central meridian; Northing — distance (km) from equator)

(Fig. 9) and a larger, positive, change in the regional regression model (Supplementary Information). The increase or decrease in areal extent changes for different NDVI values and depends on the choice of model (Table 3). We estimate changes in forest extent by looking at variations in the area with NDVI of 0.7 or above; this value coincides with the lower boundary of the xeromorphic forest. During the LGM the cooling of 4 °C results in a 20 % to 100 % increase in forest extent; the analysis shows that NDVI is more sensitive to a decrease in cloud-base height than to the combined effects of reduced rainfall, reduced atmospheric humidity, reduced CO_2 and a change in the lapse rate. This effect of cloud-base height on NDVI is largest on the south-eastern slope.

For the global warming scenario, the area with NDVI > 0.7 declines to 45 % (local regression model) or 0 % (regional regression model) of the present extent in response to a higher cloud-base height (Table 3).

Table 3: Sensitivity of surface of area with NDVI above 0.6, 0.7, and 0.8 estimated by the local and regional regression models. NDVI=0.7 corresponds to the lower extent of the xeromorphic forest. NDVI values of the upper boundary of this forest overlap with NDVI values of the sub-humid forest, a NDVI of 0.8 indicates a very dense green forest; and a NDVI of 0.6 approximately coincides with the lower limit of the open forest

		LGM		Global warming	
	Mean 2001–15	local	regional	local	regional
> 0.8	24.1 km^2	3.4 km^2	98.2 km^2	0 km^2	0 km^2
> 0.7	118.4 km^2	235.1 km^2	145.6 km^2	52.8 km^2	0 km^2
> 0.6	145.6 km^2	620.6 km^2	255.5 km^2	113.4 km^2	105.8 km^2

4. Discussion

Tropical montane forest taxa moved to lower altitudes during the LGM as the extent of tropical lowland forests contracted (Flenley, 1998; Ivory and Russell, 2016). There is therefore a unique aspect to the response of tropical montane taxa to present, past and future climatic changes. Several suggestions have been made to explain this. For example Colinvaux et al. (1996) and Flenley (1998) suggested that lower temperatures contributed to conditions suitable for the downward movement of these taxa during the LGM, whereas Flenley (1996) speculated that an altered combination of temperature and UV-B radiation might have been responsible, and Jolly and Haxeltine (1997);

Street-Perrott et al. (1997, 2007) and Izumi and Lézine (2016) emphasized the physiological impacts of reduced CO_2 at high altitudes. In contrast, Bush et al. (2011) noted an increase in the occurrence of species adapted to persistent cloud cover; cloud-forest species exhibit other adaptations as well such as microphyllous or even pachyphyllous leaves and resistance to moulds to allow them to thrive in damp conditions, and be able to cope with the alternation between near darkness during dense fog to a high solar (including UV) flux during clear intervals.

Quantifying the effects of climatic change on cloud forest vegetation has been difficult because of a lack of modern and historical data on fog capture in TMCFs. We analysed modern-day meteorological observations and satellite NDVI data of Mt Marsabit in northern Kenya to estimate the sensitivity of forest extent to climate change.

4.1. Modern day occult precipitation

We use MODIS and AVHRR NDVI data to estimate average total annual precipitation (sum of occult precipitation and rainfall) for 1982–2015 at 1700 mm with a standard error in the estimation of $\pm 265\,\mathrm{mm\ y^{-1}}$ and average annual occult precipitation at $900\,\mathrm{mm\ y^{-1}}$. Rainfall measurements of $700\,\mathrm{mm\ y^{-1}}$ are adjusted upwards by $73\,\mathrm{mm\ y^{-1}}$ to account for orographic effects. During years of unusually high rainfall (1982 and 1997) we expect to underestimate the amount of precipitation at the summit because our method can only estimate total annual precipitation up to $2000\,\mathrm{mm\ y^{-1}}$.

Validation of our results is not straightforward. Field measurements of fog capture use screens or frames that measure fog deposition in horizontal direction. These measurements from screens indicate high amounts of fog are captured, however these measurements are difficult to extrapolate to equivalent vertical precipitation amounts captured by the canopy. For example, the canopy has a much larger surface area and volume, has different surface properties and is situated further above the ground (Nicholson, 1936; Muchura et al., 2014; Cuní-Sanchez et al., 2018). Analysis of δ^2H and δ^{18}O isotope data indicates a large contribution of fog to groundwater as well, but this is difficult to quantify because of the small number of measurements, the high variability in the δ^2H and δ^{18}O composition of fog, and lack of measurements of rainfall isotopes (Ingraham and Matthews, 1988). An analysis of tropical and sub-tropical TMCFs globally shows that annual occult precipitation exceeds $1000\,\mathrm{mm\ y^{-1}}$ in areas with wind-exposed sites, high wind speeds and within the zone of maximum cloud occurrence (Bruijnzeel et al., 2011).

This situation occurs on Mt Marsabit since the south-east slope is exposed to year-round high winds transporting moisture from the Indian Ocean (Fig. 4).

The Marsabit forest is excessively green for the amount of rain it receives; based on the general relationship between rainfall and NDVI for the tropics (Fig. 5) we expect the NDVI to be half the observed value or less. Sources of error are an order of magnitude smaller and do not provide an alternative explanation (Supplementary Information). For example, one potential source of error is that rainfall amounts reported by the Marsabit weather station are too low. This appears not to be the case since we found that station measurements are similar to rain measurements made in the Marsabit forest; the difference between them is smaller than the adjustment for altitude we applied to the Marsabit rainfall data (Supplementary Information). Fog occurrence could either reduce evapotranspiration or could stimulate photosynthesis and vegetation greenness by increasing diffuse radiation which penetrates deeper into the canopy. We do find a reduction in evapotranspiration associated with the occurrence of fog but we also find reduced photosynthetic rates during fog because of a decrease in shortwave radiation absorbed by vegetation, and expect lower carbon allocation to leaves and lower NDVI compared to other parts of the tropics. These two effects associated with fog occurrence are of similar magnitude but of opposite sign and they therefore effectively cancel each other out (Supplementary Information). The residual error ($20\,\mathrm{mm\ y^{-1}}$) is much smaller than our estimate of uncertainty in occult precipitation ($265\,\mathrm{mm\ y^{-1}}$).

Analysis of partial correlations shows that variations in calculated cloud-base height (eq. 1) explain a larger proportion of variance in NDVI on the south-eastern slope of Mt Marsabit than rainfall (Fig. 9); this finding also supports a large contribution of occult precipitation to the total amount of precipitation received on Mt Marsabit. Based on these findings we conclude that the capture of fog by vegetation is the most likely explanation for the excessive greenness of the Marsabit forest.

4.2. LGM estimates of forest expansion

We estimate the sensitivity of forest extent to climatic change during the LGM with two models: a local regression model and a regional regression model (Section 3.4, see Supplementary Information for equations). In both models cloud-base height (eq. 1) descends by 500 m when surface temperature is decreased by $4\,^{\circ}\mathrm{C}$ (eq 4) and dewpoint temperature is left unchanged. Rainfall is decreased by 30 % which is representative for the LGM in East

Africa (Bonnefille and Chalié, 2000), the lapse rate is adjusted to reflect larger cooling with higher elevation (Loomis et al., 2017), atmospheric humidity at saturation is reduced by 22 % to take into account the effect of lower temperatures on atmospheric moisture content at saturation and NDVI is decreased by 20 % in response to lower atmospheric CO_2 concentrations (Los, 2013). Increased competition by C_4 plants and increased susceptibility of the forest to fire affecting the altitude of the tree line are not considered (Street-Perrott et al., 1997, 2004; Saurer et al., 2014; Frank et al., 2015; Midgley and Bond, 2015; Urban et al., 2015; Rucina et al., 2009). The direct effects of temperature on NDVI are also omitted because these are not significant in the observational record (Table 2). Furthermore, a decrease of 4 °C moves temperatures only slightly below the global optimal range for vegetation growth; we therefore expect only a small change in NDVI (Berry and Björkman, 1980). We find that NDVI values are most sensitive to the decrease in cloud-base; the associated increase in NDVI exceeds the reduction in NDVI caused by the other effects combined. As a result, we see an expansion of the area with NDVI above 0.7 by 20 % to 100 %, predominantly to lower elevations on the south-eastern slope.

Our sensitivity analysis suggests an additional mechanism to explain the downward movement of TMCF taxa in tropical Africa, Australasia and South America during the LGM (Stuijts et al., 1988; Hope and Tulip, 1994; Jolly et al., 1997; Behling, 1998; Flenley, 1998; Haberle and Maslin, 1998; Colinvaux et al., 2000; Marchant et al., 2002; Hope et al., 2004; Pickett et al., 2004; Anhuf et al., 2006; Street-Perrott et al., 2007; Rucina et al., 2009; Hessler et al., 2010; Bush et al., 2011; Lézine et al., 2013; Izumi and Lézine, 2016; Lézine et al., 2019); lower temperatures lead to a lower cloud-base height and increased occult precipitation. Temperature decreases during the LGM can therefore affect precipitation and ecosystems directly and indirectly; their direct response having a differential character as the structure and compositions of forests changed worldwide (Nolan et al., 2018). The increased importance of occult precipitation compared to rainfall found in the present study creates an environment more suitable for species adapted to capturing moisture from clouds. Regional disagreements occur with regard to the lower boundary of TMCF at the LGM (Izumi and Lézine, 2016), *e.g.* recent results obtained for Lake Bambili in western Equatorial Africa show that the upper limit of the Afromontane forest changed substantially between glacial and interglacial stages during the past 90,000 years, but the lower limit remained relatively unchanged (Lézine et al., 2019). By contrast, we find that on Mt

Marsabit the area with NDVI values above 0.7, corresponding to the current lower limit of the xeromorphic forest, is highly variable. We note that Mt Marsabit is surrounded by drylands, rather than a lowland forest, and that our findings agree with downward movement of TMCF taxa on mountains in East and Central Africa (Jolly et al., 1997; Street-Perrott et al., 2007; Rucina et al., 2009; Hessler et al., 2010; Schüler et al., 2012; Izumi and Lézine, 2016). The altitude of the summit of Mt Marsabit is too low for the upper limit of the TMCF to be to be represented, either today or at the LGM.

Subtle differences exist between the LGM simulations of the local and regional regression models (Fig, 9, Fig 1 in Supplementary Information, Table 3). The local regression model indicates a small change in NDVI at the summit of Mt Marsabit, but the area with NDVI values > 0.8 decreases substantially. The regional regression model shows an increase in area with NDVI values > 0.8 at the summit, but the expansion of the area with NDVI values between $0.6 <$ NDVI < 0.8 is smaller than in the local regression model. In both models conditions for taxa capturing water from clouds become more favourable compared to rainfall dependent taxa.

4.3. Global warming estimates of forest contraction

For the global warming scenario, NDVI values are estimated using an increase in calculated cloud-base height of 250 m; changes in NDVI from other effects are not taken into account. The area with NDVI > 0.7, which corresponds to the lower extent of the xeromorphic forest, decreases to 45 % or even 0 % of its current extent. The decline in NDVI is large on the south-eastern slope and around Marsabit village (north-east of the summit). The area around Marsabit village is affected to a large degree by humans, e.g. by land-cover change, groundwater withdrawal and selective harvesting for use as fodder for livestock (Cuní-Sanchez et al., 2018). Although we do not consider these effects, it is remarkable to see that this area shows a high sensitivity to climate change. This provides further evidence that appropriate management of the forest is needed to mitigate the adverse effects of global warming on hydrological resources; this is not only important for Mt Marsabit and but also for many other "islands in the desert" across the tropics.

Conclusion

Climate models have greater skill in reproducing temperatures than in reproducing changes in the hydrological cycle; large uncertainties exist in the simulation of precipitation, soil moisture, evapotranspiration and atmospheric humidity (The GLACE Team et al., 2004). Measurements of occult precipitation are few and highly localized. Estimates of this locally very important component of the hydrological cycle are therefore largely untested in climate simulations. The approach adopted in the present paper is one of only a few ways in which estimates of the effects of climate change on TMCFs such as that on Mt Marsabit can be obtained. Our method can be applied to other areas in the tropics with total precipitation $< 2000\,\mathrm{mm\ y^{-1}}$; the limited historical data can thus be extended to the entire period for which we have satellite data without incurring substantial costs.

The sensitivity analysis of the response of TMCFs to changes in occult precipitation and rainfall provides greater insights into the interpretation of palaeodata.

Acknowledgements

We thank the kind support given by C.O. Mahonga and the Kenya Meteorological Service for acquiring the historical rainfall and fog data from Mt Marsabit. ACS was funded by Marie Curie Actions Intra-European Fellowships (IEF), Number 328075. The British Institute in Eastern Africa are thanked for ongoing logistical help during fieldwork around Mt Marsabit

Bibliography

Aerts, R., Geeraert, L., Berecha, G., Hundera, K., Muys, B., De Kort, H., Honnay, O., 2017. Conserving wild Arabica coffee: Emerging threats and opportunities. Agric., Ecosyst. Environ. 237, 75–79.

Anhuf, D., Ledru, M., Behling, H., Da Cruz Jr, F. W., Cordeiro, R. C., Van der Hammen, T., Karmann, I., Marengo, J. A., De Oliveira, P. E., Siffedine, A., Albuquerque, A. L., Da Silva Dias, P. L., 2006. Paleo-environmental change in Amazonian and African rainforest during the LGM. Palaeogeogr. Palaeocl. 239, 510–527, doi: 10.1016/j.palaeo.2006.01.017.

Behling, H., 1998. Late Quaternary vegetational and climatic changes in Brazil. Rev. Palaeobot. Palyno. 99, 143–156, doi: 10.1016/S0034–6667(97)00044–4.

Berrisford, P., Dee, D., Poli, P., Brugge, R., Fielding, K., Fuentes, M., Kallberg, P., Kobayashi, S., Uppala, S., Simmons, A., 2011. The ERA-Interim archive Version 2.0, ERA Report Series 1. ECMWF, Shinfield Park, Reading, United Kingdom.

Berry, J., Björkman, O., 1980. Photosynthetic response and adaptation to temperature in higher plants. Annu. Rev. Plant Physiol. 31, 491–543.

Bonnefille, R., Chalié, F., 2000. Pollen-inferred precipitation time-series from equatorial mountains, Africa, the last 40 kyr BP. Global Planet. Change 26, 25–50, doi: 10.1016/S0921–8181(00)00032–1.

Bonnefille, R., Roeland, J. C., Guiot, J., 1990. Temperature and rainfall estimates for the past 40,000 years in equatorial Africa. Nature 346, 347–349, doi: 10.1038/346347a0.

Boom, A., Mora, G., Cleef, A. M., Hooghiemstra, H., 2001. High altitude C_4 grasslands in the northern Andes: relicts from glacial conditions? Rev. Palaeobot. Palyno. 115, 147–160, doi: 10.1016/S0034–6667(01)00056–2.

Bradley, R. S., Keimig, F. T., Diaz, H. F., 2004. Projected temperature changes along the American cordillera and the planned GCOS network. Geophys. Res. Lett. 31, L16210, doi: 10.1029/2004GL020229.

Bruijnzeel, L. A., Mulligan, M., Scatena, F. N., 2011. Hydrometeorology of tropical montane cloud forests: emerging patterns. Hydrol. Process. 25, 465–498, doi: 10.1002/hyp.7974.

Bruijnzeel, L. A., Proctor, J., 1995. Hydrology and biogeochemistry of tropical montane cloud forests: what do we really know. In: Hamilton, L. S., Juvik, J. O., Scatena, F. N. (Eds.), Tropical Montane Cloud Forests. Vol. 110. Springer Verlag, New York, pp. 38–78.

Bruijnzeel, L. A., Scatena, F. N., Hamilton, L. S., 2010. Tropical Montane Cloud Forests. Science for Conservation and Management. Cambridge University Press, Cambridge, UK.

Bush, M. B., Hanselman, J. A., Hooghiemstra, H., 2011. Andean montane forests and climate change, 2nd Edition. Springer-Verlag, Berlin Heidelberg, Tropical Rainforest Responses to Climatic Change Chapter 2, pp. 35–60.

Bussmann, R. W., 2002. Islands in the desert — Forest vegetation of Kenya's smaller mountains and highland areas (Nyiru, Ndoto, Kulal, Marsabit, Loroghi, Ndare, Mukogodo, Porror, Mathews, Gakoe, Imenti, Ngaia, Nyambeni, Loita, Nguruman, Nairobi). J. East Afr. Nat. Hist. 91, 27–79.

Cavelier, J., 1996. Tropical Forest Plant Ecophysiology. No. 14. International Thomson Publishing, Florence, Kentucky 41042, USA, Ch. Environmental factors and ecophysiological processes along altitudinal gradients in wet tropical mountains, pp. 399–439, doi: 10.1007/978–1–4613–1163–8_14.

Chapin, F., 1980. The mineral nutrition of wild plants. Ann. Rev. Ecol. and Syst. 11, 233–260.

Colinvaux, P. A., De Oliveira, P. E., Bush, M. B., 2000. Amazonian and neotropical plant communities on glacial time scales: The failure of the aridity and refuge hypotheses. Quaternary Sci. Rev. 19, 141–169.

Colinvaux, P. A., Moreno, J. E., Bush, M. B., 1996. A long pollen record from lowland Amazonia: Forest and cooling in glacial times. Science 274, 85–88, doi: 10.1126/science.274.5284.85.

Cowling, S. A., Maslin, M. A., Sykes, M. T., 2001. Paleovegetation simulations of lowland Amazonia and implications for neotropical allopatry and speciation. Quaternary Res. 55, 140–149, doi: 10.1006/qres.2000.2197.

Cuní-Sanchez, A., Omeney, P., Pfeifer, M., Olaka, L., Boru Mamo, M., Marchant, R., Burgess, N. D., 2018. Climate change and pastoralists: perceptions and adaptation in montane Kenya. Clim. Dev., 1–12, doi: 10.1080/17565529.2018.1454880.

Dabasso, B. H., Okomoli, M. O., 2015. Changing pattern of local rainfall: analysis of a 50-year record in central Marsabit, northern Kenya. Weather 70, 285–289.

Diaz, H. F., Bradley, R. S., Ning, L., 2014. Climatic changes in mountain regions of the American Cordillera and the tropics: historical changes and

future outlook. Arctic Ant. Alp. Res. 46, 735–743, doi: 10.1657/1938–4246–46.4.735.

Farrera, I., Harrison, S. P., Prentice, I. C., Ramstein, G., Guiot, J., Bartlein, P. J., Bonnefille, R., Bush, M., Cramer, W., von Grafenstein, U., Holmgren, K., Hooghiemstra, H., Hope, G., Dolly, D., Lauritzen, S. E., Ono, Y., Pinot, S., Stute, M., Yu, G., 1999. Tropical climates at the Last Glacial Maximum: a new synthesis of terrestrial palaeoclimate data. i. vegetation, lake-levels and geochemistry. Clim. Dynam. 15, 823–856, doi: 10.1007/s003820050317.

Flenley, J. R., 1996. Problems of the Quaternary on mountains of the Sunda-Sahul region. Quaternary Sci. Rev. 15, 549–555, doi: 10.1016/0277–3791(96)00017–0.

Flenley, J. R., 1998. Tropical forests under the climates of the last 30,000 years. Climatic Change 39, 177–197, doi: 10.1023/A:1005367822750.

Foerster, V., Vogelsang, R., Junginger, A., Asrat, A., Lamb, H. F., Schaebitz, F., Trauth, M. H., 2015. Environmental change and human occupation of southern Ethiopia and northern Kenya during the last 20,000 years. Quaternary Sci. Rev. 129, 333–340, doi: 10.1016/j.quascirev.2015.10.026.

Foster, P., 2001. The potential negative impact of global climate change on tropical montane cloud forest. Earth Sci. Rev. 55, 73–106.

Frank, D. C., Poulter, B., Saurer, M., Esper, J., Huntingford, C., Helle, G., Treydte, K., Zimmermann, N. E., Schleser, G. H., Ahlstrom, A., Ciais, P., Friedlingstein, P., Levis, S., Lomas, M., Sitch, S., Viovy, N., Andreu-Hayles, L., Bednarz, Z., Berninger, F., Boettger, T., D'Alessandro, C. M., Daux, V., Filot, M., Grabner, M., Gutierrez, E., Haupt, M., Hilasvuori, E., Jungner, H., Kalela-Brundin, M., Krapiec, M., Leuenberger, M., Loader, N. J., Marah, H., Masson-Delmotte, V., Pazdur, A., Pawelczyk, S., Pierre, M., Planells, O., Pukiene, R., Reynolds-Henne, C. E., Rinne, K. T., Saracino, A., Sonninen, E., Stievenard, M., Switsur, V. R., Szczepanek, M., Szychowska-Krapiec, E., Todaro, L., Waterhouse, J. S., Weigl, M., 06 2015. Water-use efficiency and transpiration across european forests during the anthropocene. Nat. Clim. Change 5, 579–583, doi: 10.1038/nclimate2614.

Fu, Q., Manabe, S., Johanson, C. M., 2011. On the warming in the tropical upper troposphere: Model versus observations. Geophys. Res. Lett. 38, L15704, doi:10.1029/2011GL048101.

Githae, E. W., Chuah-Petiot, M., Mworia, J. K., Odee, D. W., 2007. A botanical inventory and diversity assessment of Mt. Marsabit forest, a sub-humid montane forest in the arid lands of northern Kenya. African J. Ecology 46, 39–45, doi: 10.1111/j.1365–2028.2007.00805.x.

Grubb, P. J., 1977. The maintenance of species-richness in plant communities: the importance of the regeneration niche. Biological Reviews 52, 107–145.

Grubb, P. J., Whitmore, T. C., 1966. A comparison of montane and lowland rain forets in Ecuador: II. The climate and its effects on the distribution and physiognomy of the forests. J. Ecology 54, 303–333, doi: 10.2307/2257951.

Haberle, S. G., Maslin, M. A., 1998. Late Quaternary vegetation and climate change in the Amazon basin based on a 50,000 year pollen record from the Amazon fan, ODP site 932. Quaternary Res. 51, 27–38, doi: 10.1006/qres.1998.2020.

Hamilton, A. C., 1982. Environmental history of East Africa: a study of the Quaternary. Academic Press, London, United Kingdom.

Harris, I., Jones, P. D., Osborn, T. J., Lister, D. H., 2014. Updated high-resolution grids of monthly climatic observations – the CRU TS3.10 dataset. Int. J. Climatol. 34, 623–712, doi: 10.1002/joc.3711.

Helmer, E. H., Gerson, E. A., Scott Baggett, L., Bird, B. J., Ruzycki, S., Vogesser, S. M., 2019. Neotropical cloud forests and páramo to contract and dry from declines in cloud immersion and frost. PLOS ONE, e0213155 doi: 10.1371/journal.pone.0213155.

Hemp, A., 2009. Climate change and its impact on the forests of Kilimanjaro. African J. Ecology 47, 3–10, doi: 10.1111/j.1365–2028.2008.01043.x.

Hessler, I., Dupont, L., Bonnefille, R., Behling, H., González, C., Helmens, K. F., Hooghiemstra, H., Lebamba, J., Ledru, M.-P., Lézine, A.-M., Maley, J., Marret, F., Vincens, A., 2010. Millennial-scale changes in vegetation

records from tropical Africa and South America during the last glacial. Quaternary Sci. Rev. 29, 2882–2899, doi: 10.1016/j.quascirev.2009.11.029.

Hope, G., Kershaw, A. P., Van der Kaars, S., Xiangjun, S., Liew, P.-M., Heusser, L. E., Takahara, H., McGlone, M., Miyoshi, N., Moss, P. T., 2004. History of vegetation and habitat change in the austral-asian region. Quaternary Int. 118–119, 103–126, doi: 10.1016/S1040–6182(03)00133–2.

Hope, G., Tulip, J., 1994. A long vegetation history from lowland Irian Jaya, Indonesia. Palaeogeogr. Palaeocl. 109, 385–398, doi: 10.1016/0031–0182(94)90187–2.

Hostetler, S. W., Clark, P. U., 2000. Tropical climate at the Last Glacial Maximum inferred from glacier mass-balance modeling. Science 290, 1747–1750, doi: 10.1126/science.290.5497.1747.

Huete, A., Didan, K., Miura, T., Rodriguez, E. P., Gao, X., Ferreira, L. G., 2002. Overview of the radiometric and biophysical performance of the modis vegetation indices. Remote Sens. Environ. 83, 195–213.

Huffman, G. J., Adler, R. F., Bolvin, D. T., Gu, G., Nelkin, E. J., Bowman, K. P., Hong, Y., Stocker, E. F., Wolff, D. B., 2007. The TRMM multi-satellite precipitation analysis: Quasi-global, multi-year, combined-sensor precipitation estimates at fine scale. J. Hydrometeorology 8, 38–55, doi: 10.1175/JHM560.1.

Huffman, G. J., Adler, R. F., Bolvin, D. T., Nelkin, E. J., 2010. Satellite Rainfall Applications for Surface Hydrology. Springer Verlag, Heidelberg, Germany, Ch. 1. The TRMM Multi-satellite Precipitation Analysis (TMPA), doi: 10.1007/978-90-481-2915-7.

Ingraham, N. L., Matthews, R. A., 1988. Fog drip as a source of groundwater recharge in Northern Kenya. Water Resources Research 24, 1406–1410.

IPCC, 2013. Climate Change 2013: The Physical Science Basis. Working Group I Contribution to the Fifth Assessment Report of the Intergovernmental Panel on Climate Change. Cambridge University Press, Cambridge, UK.

IUCN, 2016. The IUCN red list of threatened species. Version 2016.3 available from www.iucnredlist.org.

Ivory, S. J., Russell, J., 2016. Climate, herbivory and fire controls on tropical african forest for the last 60ka. Quaternary Sci. Rev. 148, 101–114, doi: 10.1016/j.quascirev.2016.07.015.

Izumi, K., Lézine, A.-M., 2016. Pollen-based biome reconstructions over the past 18,000 years and atmospheric co_2 impacts on vegetation in equatorial mountains of Africa. Quaternary Sci. Rev. 152, 93–103, doi: 10.1016/j.quascirev.2016.09.023.

James, M. E., Kalluri, S. N. V., 1994. The Pathfinder AVHRR Land data set - an improved coarse resolution data set for terrestrial monitoring. Int. J. Remote Sens. 15 (17), 3347–3363.

Jarvis, A., Reuter, H. I., Nelson, A., Guevara, A., 2008. Hole-filled SRTM for the globe version 4, available from the CGIAR-CSI SRTM 90m database. http://srtm.csi.cgiar.org.

Jolly, D., Haxeltine, A., 1997. Effect of low glacial atmospheric CO_2 on tropical African montane vegetation. Science 276, 786–787.

Jolly, D., Taylor, D., Marchant, R., Hamilton, A., Bonnefille, R., Buchet, G., Riollet, G., 1997. Vegetation dynamics in central Africa since 18,000 yr BP: pollen records from the interlacustrine highlands of Burundi, Rwanda and western Uganda. J. Biogeogr. 24, 495–512, doi: 10.1111/j.1365–2699.1997.00182.x.

Jones, H. G., 1992. Plants and microclimate: a quantitative approach to environmental plant physiology, 2nd Edition. Cambridge University Press, Cambridge, UK.

Junginger, A., Trauth, M. H., 2013. Hydrological constraints of paleo-Lake Suguta in the Northern Kenya Rift during the African Humid Period (15–5 ka BP). Global Planet. Change 111, 174–188, doi: 10.1016/j.gloplacha.2013.09.005.

Karmalkar, A. V., Bradley, R. S., Diaz, H. F., 2008. Climate change scenario for Costa Rican montane forests. Geophys. Res. Lett. 35, L11702, doi: 10.1029/2008GL033940.

Kinuthia, J. H., Asnani, G. C., 1982. A newly found jet in north Kenya (Turkana Channel). Mon. Weather Rev. 110, 1722–1728, doi: 10.1175/1520–0493(1982)110<1722:ANFJIN>2.0.CO;2.

Klein Goldewijk, K., Beusen, A., Van Drecht, G., De Vos, M., 2010. The HYDE 3.1 spatially explicit database of human-induced global land-use change over the past 12,000 years. Global Ecol. Biogeogr., doi: 10.1111/j.1466–8238.2010.00587.x.

Kumar, M., Monteith, J. L., 1982. Plants and the Daylight Spectrum. Academic Press, Ch. Remote sensing of plant growth.

Lawrence, M. G., 2005. The relationship between relative humidity and the dewpoint temperature in moist air: A simple conversion and applications. B. Am. Meteorol. Soc. 86, 225–233, doi: 10.1175/BAMS–86–2–225.

Ledru, M., Bertaux, J., Sifeddine, A., Suguio, K., 1998. Absence of Last Glacial Maximum records in lowland tropical forests. Quaternary Res. 49, 233–237, doi: 10.1006/qres.1997.1953.

Lézine, A. M., Assi-Kaudjhis, C., Roche, E., Vincens, A., Achoundon, G., 2013. Towards an understanding of West African montane forest response to climate change. J. Biogeogr. 40, 183–196.

Lézine, A. M., Izumi, K., Kageyama, M., Achoundon, G., 2019. A 90,000-year record of Afromontane forest responses to climate change. Science 363, 177–181.

Lister, B. C., Garcia, A., 2018. Climate-driven declines in arthropod abundance restructure a rainforest food web. P. Natl. Acad. Sci. USA 115, E10397–E10406, doi: 0.1073/pnas.1722477115.

Loomis, S., Russell, J., Verschuren, D., Morrill, C., De Cort, G., Sinninghe Damsté, J., Olago, D., Eggermont, H., Street-Perrott, F., Kelly, M., 2017. The tropical lapse rate steepened during the last glacial maximum. Science Advances 3, e1600815, doi: 10.1126/sciadv.1600815.

Los, S. O., 1998. Estimation of the ratio of sensor degradation between NOAA AVHRR channels 1 and 2 from monthly NDVI composites. IEEE T. Geosci. Remote 36, 206–213.

Los, S. O., 2013. Analysis of trends in fused AVHRR and MODIS NDVI data for 1982–2006: Indication for a CO_2 fertilization effect in global vegetation. Global Biogeochem. Cy. 27, 318–330, doi: 10.1002/gbc.20027.

Los, S. O., Collatz, G. J., Bounoua, L., Sellers, P. J., Tucker, C. J., 2001. Global interannual variations in sea surface temperature and land surface vegetation, air temperature, and precipitation. J. Climate 14, 1535–1549.

Los, S. O., Collatz, G. J., Sellers, P. J., Malmstrom, C. M., Pollack, N. H., DeFries, R. S., Bounoua, L., Parris, M. T., Tucker, C. J., Dazlich, D. A., 2000. A global 9-yr biophysical land surface dataset from NOAA AVHRR data. J. Hydrometeorology 1, 183–199.

Los, S. O., North, P. R. J., Grey, W. M. F., Barnsley, M. J., 2005. A method to convert AVHRR normalized difference vegetation index time series to a standard viewing and illumination geometry. Remote Sens. Environ. 99, 400–411, doi: 10.1016/j.rse.2005.08.017.

Maley, J., 1987. Palaeoecology of Africa and the surrounding islands. Balkema, Rotterdam – the Netherlands, Brookfield – Vermont – USA, Ch. Fragmentation de la forêt dense humide africaine et extension des biotopes montagnards au Quaternaire récent: Nouvelles données polliniques et chronologiques. Implications paléoclimatiques et biogéographiques.

Maley, J., 1989. Paleoclimatology and paleometeorology: Modern and past patterns of global atmospheric transport. Vol. 282 of NATO ASI Series, Series C: Mathematical and Physical Sciences. Kluwer Academic, Dordrecht – the Netherlands, Boston – USA, London – UK, Ch. Late Quaternary climatic changes in the African rain forest: forest refugia and the major rôle of sea surface temperature variations.

Marchant, R., Behling, H., Berrio, J.-C., Cleef, A., Duivenvoorden, J., Hooghiemstra, H., Kuhry, P., Melief, B., Schreve-Brinkman, E., Van Geel, B., Van der Hammen, T., Van Reenen, G., Wille, M., 2002. Pollen-based biome reconstructions for Colombia at 3000, 6000, 9000, 12 000, 15 000 and 18 000 ^{14}C yr ago: Late Quaternary tropical vegetation dynamics. J. Quaternary Science 17, 113–129, doi: 10.1002/jqs.669.

Marchant, R., Mumbi, C., Behera, S., Yamagata, T., 2006. The Indian Ocean dipole — the unsung driver of climatic variability in East Africa. African J. Ecology 45, 4–16, doi: 10.1111/j.1365–2028.2006.00707.x.

Martínez, M. L., Pérez-Maqueo, O., Vázquez, G., Castillo-Campos, G., García-Franco, J., Mehltreter, K., Equihua, M., Landgrave, R., 2009. Effects of land use change on biodiversity and ecosystem serices in tropical montane cloud forests of Mexico. Forest Ecol. Manage. 258, 1856–1863, doi: 10.1016/j.foreco.2009.02.023.

Midgley, G. F., Bond, W. J., 2015. Future of African terrestrial biodiversity and ecosystems under anthropogenic climate change. Nature Clim. Change 5, 823–829, doi: 10.1038/nclimate2753.

Mittermeier, R. A., Robles, G. P., Lamoreux, J., da Fonseca, G. A. B., 2004. Hotspots revisited. Tech. rep., CEMEX, Garzia Garcia N. L. Mexico.

Moat, J., Gole, T. W., Davis, A. P., 2019. Least concern to endangered: Applying climate change projections profoundly influences the extinction risk assessment for wild Arabica coffee. Glob. Change Biol. 25, 390–403, doi: 10.1111/gcb.14341.

Moat, J., O'Sullivan, R. J., Gole, T., Davis, A. P., 2018. *Coffea arabica*. The IUCN Red List of Threatened Species 2018: e.T18289789a18539365. Tech. Rep. doi: 10.2305/IUCN.UK.2018-2.RLTS.T18289789A18539365.en, IUCN.

Moat, J., Williams, J., Baena, S., Wilkinson, T., Gole, T. W., Challa, Z. K., Demissew, S., Davis, A. P., 06 2017. Resilience potential of the Ethiopian coffee sector under climate change. Nat. Plants 3, 17081 EP –, doi: 10.1038/nplants.2017.81.

Morrissey, A., Scholz, C. A., 2014. Paleohydrology of Lake Turkana and its influence on the Nile River system. Palaeogeogr. Palaeocl. 403, 88–100, doi: 10.1016/j.palaeo.2014.03.029.

Muchura, H. M., Min, S. C., Mworia, J. K., Gichuki, N. N., 2014. Role of Bryophytes and tree canopy in mist trapping in Mt. Marsabit forest. J. Environ. Earth Sci. 4, 128–139.

Myneni, R. B., Keeling, C. D., Tucker, C. J., Asrar, G., Nemani, R. R., 1997. Increased plant growth in the northern high latitudes from 1981 to 1991. Nature 386, 698–702.

Myneni, R. B., Los, S. O., Tucker, C. J., 1996. Satellite-based identification of linked vegetation index and sea surface temperature anomaly areas from 1982–1990 for Africa, Australia and South America. Geophys. Res. Lett. 23, 729–732, doi: 10.1029/96GL00266.

Ngene, S. M., Van Gils, H., Van Wieren, S. E., Rasmussen, H., Skidmore, A. K., Prins, H. H. T., Toxopeus, A. G., Omondi, P., Douglas-Hamilton, I., 2010. The ranging patterns of elephants in Marsabit protected area, Kenya: the use of satellite-linked GPS collars. African J. Ecol. 48, 386–400, doi: 10.1111/j.1365–2028.2009.01125.x.
URL http://dx.doi.org/10.1111/j.1365-2028.2009.01125.x

Nicholson, J. W., 1936. The influence of forests on climate and water supply in Kenya. East African Agric. Forest. J. 48–53 (164–170), 226–240.

Nolan, C., Overpeck, J. T., Allen, J. R. M., Anderson, P. M., Betancourt, J. L., Binney, H. A., Brewer, S., Bush, M. B., Chase, B. M., Cheddadi, R., Djamali, M., Dodson, J., Edwards, M. E., Gosling, W. D., Haberle, S., Hotchkiss, S. C., Huntley, B., Ivory, S. J., Kershaw, A. P., Kim, S.-H., Latorre, C., Leydet, M., Lézine, A.-M., Liu, K.-B., Liu, Y., Lozhkin, A. V., McGlone, M. S., Marchant, R. A., Momohara, A., Moreno, P. I., Müller, S., Otto-Bliesner, B. L., Shen, C., Stevenson, J., Takahara, H., Tarasov, P. E., Tipton, J., Vincens, A., Weng, C., Xu, Q., Zheng, Z., Jackson, S. T., 2018. Past and future global transformation of terrestrial ecosystems under climate change. Science 361, 920–923, doi: 10.1126/science.aan5360.

O'Gorman, P. A., Singh, M. S., 2013. Vertical structure of warming consistent with an upward shift in the middle and upper troposphere. Geophys. Res. Lett. 40, 1838–1842, doi: 10.1002/grl.50328.

Ohmura, A., 2012. Enhanced temperature varaibility in high-altitude climate change. Theor. Appl. Climatol. 110, 499–508, doi: 10.1007/s00704–012–0687–x.

Oliveira, R. S., Eller, C. B., Bittencourt, P. R. L., Mulligan, M., 2014. The hydroclimatic and ecophysiological basis of cloud forest distributions under current and projected climates. Ann. Bot.-London 113, 909–920, doi: 10.1093/aob/mcu060.

Perrott, R. A., Street-Perrott, F. A., 1982. New evidence for a Late Pleistocene wet phase in northern intertropical Africa. Palaeoecol. Africa 14, 57–75.

Pickett, E. J., Harrison, S. P., Hope, G., Harle, K., Dodson, J. R., Peter Kershaw, A., Colin Prentice, I., Backhouse, J., Colhoun, E. A., D'Costa, D., Flenley, J., Grindrod, J., Haberle, S., Hassell, C., Kenyon, C., Macphail, M., Martin, H., Martin, A. H., McKenzie, M., Newsome, J. C., Penny, D., Powell, J., Ian Raine, J., Southern, W., Stevenson, J., Sutra, J.-P., Thomas, I., Van der Kaars, S., Ward, J., 2004. Pollen-based reconstructions of biome distributions for Australia, Southeast Asia and the Pacific (SEAPAC region) at 0, 6000 and 18,000 ^{14}C yr BP. J. Biogeogr. 31, 1381–1444, doi:10.1111/j.1365–2699.2004.01001.x.

Pounds, J. A., Fogden, M. P. L., Campbell, J. H., 1999. Biological response to climate change on a tropical mountain. Nature 398, 611–615, doi: 10.1038/19297.

Prentice, I. C., Harrison, S. P., 2009. Ecosystem effects of CO_2 concentration: evidence from past climates. Clim. Past 5, 297–307, doi: 10.5194/cp–5–297–2009.

Prince, S. D., 1991. Satellite remote sensing of primary production: comparison of results for Sahelian grasslands 1981–1988. Int. J. Remote Sens. 12, 1301–1311.

Rucina, S. M., Muiruri, V. M., Kinyanjui, R. N., McGuiness, K., Marchant, R., 2009. Late Quaternary vegetation and fire dynamics on Mount Kenya. Palaeogeogr. Palaeocl. 283, 1–14.

Ryan, M. G., 1991. Effects of climate change on plant respiration. Ecol. Appl. 1, 157–167.

Saurer, M., Spahni, R., Frank, D. C., Joos, F., Leuenberger, M., Loader, N. J., McCarroll, D., Gagen, M., Poulter, B., Siegwolf, R. T., Andreu-Hayles, L., Boettger, T., Dorado Liñán, I., Fairchild, I. J., Friedrich, M., Gutierrez, E., Haupt, M., Hilasvuori, E., Heinrich, I., Helle, G., Grudd, H., Jalkanen, R., Levanič, T., Linderholm, H. W., Robertson, I., Sonninen, E., Treydte, K., Waterhouse, J. S., Woodley, E. J., Wynn, P. M., Young, G. H.,

2014. Spatial variability and temporal trends in water-use efficiency of european forests. Glob. Change Biol. 20, 3700–3712, doi: 10.1111/gcb.12717.

Scatena, F. N., Bruijnzeel, L. A., Bupp, P., Das, S., 2010. Tropical Montane Cloud Forests. Science for Conservation and Management. No. 1. Cambridge University Press, Cambridge, UK, Ch. Setting the stage.

Schüler, L., Hemp, A., Zech, W., Behling, H., 2012. Vegetation, climate and fire-dynamics in East Africa inferred from the Maundi crater pollen record from Mt Kilimanjaro during the last glacial-interglacial cycle. Quaternary Sci. Rev. 39, 1–13, doi: 10.1016/j.quascirev.2012.02.003.

Smith, A. N., Lott, N., Vose, R., 2011. The integrated surface data base: Recent developments and partnerships. B. Am. Meteorol. Soc. 92, 704–708, doi:10.1175/2011BAMS3015.1.

Stager, J. C., Anfang-Sutter, R., 1999. Preliminary evidence of environmental changes at Lake Bambili (Cameroon, West Africa) since 24,000 BP. J. Paleolimnology 22, 319–330, doi: 10.1023/A:1008098211671.

Still, C. J., Foster, P. N., Schneider, S. H., 1999. Simulating the effects of climate change on tropical montane forests. Nature 389, 608–610.

Street-Perrott, F. A., Barker, P. A., Swain, D. L., Ficken, K. J., Wooller, M. J., Olago, D. O., Huang, Y., 2007. Late Quaternary changes in ecosystems and carbon cycling on Mt. Kenya, East Africa: a landscape-ecological perspective based on multi-proxy lake-sediment influxes. Quaternary Sci. Rev. 26, 1838–1860, doi: 10.1016/j.quascirev.2007.02.014.

Street-Perrott, F. A., Ficken, K. J., Huang, Y., Eglinton, G., 2004. Late Quaternary changes in carbon cycling on Mt. Kenya, East Africa: an overview of the δ^{13}C record in lacustrine organic matter. Quaternary Sci. Rev. 23, 861–879, doi: 10.1016/j.quascirev.2003.06.007.

Street-Perrott, F. A., Huang, Y., Perrott, R. A., Eglington, G., Barker, P., Ben Khelifa, L., Harkness, D. D., Olago, D. O., 1997. Impact of lower atmospheric carbon dioxide on tropical mountain ecosystems. Science 278, 1422–1424, doi: 10.1126/science.278.5342.1422.

Stuijts, I., Newsome, J. C., Flenley, J. R., 1988. Evidence for late quaternary vegetational change in the Sumatran and Javan highlands. Rev. Palaeobot. Palyno. 55, 207–216, doi: 10.1016/0034–6667(88)90086–3.

The GLACE Team, Koster, R. D., Dirmeyer, P. A., Guo, Z., Bonan, G., Chan, E., Cox, P., Gordon, C. T., Kanae, S., Kowalczyk, E., Lawrence, D., Liu, P., Lu, C.-H., Malyshev, S., McAvaney, B., Mitchell, K., Mocko, D., Oki, T., Oleson, K., Pitman, A., Sud, Y. C., Taylor, C. M., Verseghy, D., Vasic, R., Xue, Y., Yamada, T., 2004. Regions of strong coupling between soil moisture and precipitation. Science 305, 1138–1140, doi: 10.1126/science.1100217.

Tucker, C. J., Dregne, H. E., Newcomb, W. W., 1991. Expansion and contraction of the Sahara desert from 1980 to 1990. Science 253, 299–301.

Tucker, C. J., Justice, C. O., Prince, S. D., 1986. Monitoring the grasslands of the Sahel 1984–1985. Int. J. Remote Sens. 7, 1571–1582.

Urban, M. A., Nelson, D. M., Street-Perrott, F. A., Verschuren, D., Hu, F. S., 2015. A late-Quaternary perspective on atmospheric pCO_2, climate, and fire as drivers of C_4-grass abundance. Ecology 96, 642–653, doi: 10.1890/14–0209.1.

Urrego, D. H., Bush, M. B., Silman, M. R., 2010. A long history of cloud and forest migration from Lake Consuelo, Peru. Quaternary Res. 73, 364–373, doi: 10.1016/j.yqres.2009.10.005.

Van Zinderen-Bakker, E. M., Coetzee, J. A., 1972. A re-appraisal of late-Quaternary climatic evidence from tropical Africa. Palaeoecol. Africa 7, 151–181.

Vizy, E. K., Cook, K. H., 2007. Relationship between Amazon and high Andes rainfall. J. Geophys. Res. 112, D07107, doi: 10.1029/2006JD007980.

Webb III, T., Ruddiman, W. F., Street-Perrott, F. A., Markgraf, V., Kutzbach, J. E., Bartlein, P. J., Wright Jr, H. E., Prell, W. L., 1993. Global Climates since the Last Glacial Maximum. University of Minnesota Press, Ch. Climatic changes during the past 18,000 years: Regional syntheses, mechanisms and causes, pp. 514–535.

Williams, J. W., Jackson, S. T., Kutzbach, J. F., 2007. Projected distributions of novel and disappearing climates by 2100 AD. Proc. Natl. Acad. Sci. USA 104, 5738–5742, doi: 10.1073/pnas.0606292104.

Wooller, M. J., Street-Perrott, F. A., Agnew, A. D. Q., 2000. Late Quaternary fires and grassland palaeoecology of Mount Kenya, East Africa: evidence from charred grass cuticles in lake sediments. Palaeogeogr. Palaeocl. 164, 207–230, doi: 10.1016/S0031–0182(00)00187–5.

Wu, H., Guiot, J., Brewer, S., Guo, Z., Peng, C., 2007. Dominant factors controlling glacial and interglacial variations in the treeline elevation in tropical Africa. P. Natl. Acad. Sci. USA 104, 9720–9724, doi: 10.1073/pnas.0610109104.

Zhu, Z., Piao, S., Myneni, R. B., Huang, M., Zeng, Z., Canadell, J. G., Ciais, P., Sitch, S., Friedlingstein, P., Arneth, A., Cao, C., Cheng, L., Kato, E., Koven, C., Li, Y., Lian, X., Liu, Y., Liu, R., Mao, J., Pan, Y., Peng, S., Peñuelas, J., Poulter, B., Pugh, T. A. M., Stocker, B. D., Viovy, N., Wang, X., Wang, Y., Xiao, Z., Yang, H., Zaehle, S., Zeng, N., 04 2016. Greening of the earth and its drivers. Nature Clim. Change 6, 791 EP –, doi:10.1038/nclimate3004.